

Energy & Environmental Science

Accepted Manuscript



This is an *Accepted Manuscript*, which has been through the Royal Society of Chemistry peer review process and has been accepted for publication.

Accepted Manuscripts are published online shortly after acceptance, before technical editing, formatting and proof reading. Using this free service, authors can make their results available to the community, in citable form, before we publish the edited article. We will replace this *Accepted Manuscript* with the edited and formatted *Advance Article* as soon as it is available.

You can find more information about *Accepted Manuscripts* in the [Information for Authors](#).

Please note that technical editing may introduce minor changes to the text and/or graphics, which may alter content. The journal's standard [Terms & Conditions](#) and the [Ethical guidelines](#) still apply. In no event shall the Royal Society of Chemistry be held responsible for any errors or omissions in this *Accepted Manuscript* or any consequences arising from the use of any information it contains.

Cite this: DOI: 10.1039/c0xx00000x

www.rsc.org/xxxxxx

Review

Theory, practice and prospects of x-ray and neutron scattering for lignocellulosic biomass characterization: towards understanding biomass pretreatment

Gang Cheng,^{*a} Xin Zhang^a, Blake Simmons^{b,c} and Seema Singh^{*b,c}

Received (in XXX, XXX) Xth XXXXXXXXX 20XX, Accepted Xth XXXXXXXXX 20XX
Received (in XXX, XXX) Xth XXXXXXXXX 20XX, Accepted Xth XXXXXXXXX 20XX

DOI: 10.1039/b000000x

Abstract: Efficient deconstruction of lignocellulosic biomass into fermentable sugar depends largely on the development of advanced biomass pretreatment technologies. Due to the highly heterogeneous nano- and microstructure of the plant cell walls, there is a lack of understanding with regards to interactions between biomass recalcitrance and biomass pretreatment. Progresses have been made by comparing the changes in chemical compositions and physical structures during pretreatment processes and their correlations with the enzymatic hydrolysis of pretreated biomass. Recent studies suggest the necessity of investigating impacts of biomass pretreatment on plant cell walls using analytical tools spanning multiple length scales. Scattering techniques including x-ray and neutron scattering, complementary to imaging techniques, offer several advantages like minimum sample preparation, versatile sample environment and in situ dynamic investigation of cell wall structures. The combination of wide and small angle scattering (WAS and SAS) techniques covers length scales from a few angstroms to several hundred nano-meters. In this review article, a detailed overview of application of WAS and SAS techniques to study the supramolecular structures of cellulose and lignin and, examination of the presence of pores in plant cell walls as well as in the cellulose fibres are presented. In-situ enzymatic hydrolysis of cellulose investigated by SAS, providing important insight into enzyme-biomass interactions, are also summarized. This review highlights how probing structural changes during pretreatment of biomass samples by WAS and SAS can reveal valuable information that are often not accessible by other techniques.

Broader context: Lignocellulosic biomass is of particular interest as a sustainable source of sugars and platform chemicals for conversion into renewable fuels, chemicals and materials. However, biomass must be pre-treated to overcome recalcitrance and allow for enzyme accessibility to cellulose and maximize product recovery for improved economics of second-generation lignocellulosic bio-refinery. Interest and efforts on the production of fuels and chemicals from lignocellulosic biomass is growing rapidly and by analyzing recent research progresses in this field, more knowledge can be gained about the applied aspect of different pretreatment technologies. The complex interactions between plant cell walls and biomass pretreatment generate recalcitrance-related structural changes on multiple length scales. Recent research activities in understanding biomass pretreatment have been shifting from cell wall chemistry to reorganization/redistribution of cell wall components: cellulose, hemicelluloses and lignin. A deeper understanding of biomass recalcitrance requires application of analytical tools spanning multiple length scales. There has been an increasing number of publications over the past two years, which have taken advantage of wide and small angle scattering tools to understand structural changes during pretreatment of biomass samples. The results of these studies are encouraging since important information is revealed which is advancing our understanding of biomass pretreatment and recalcitrance. Here we provide an overview of the theory, current practice and future prospects of WAS and SAS scattering techniques for probing lignocellulosic biomass structures with an emphasis on understanding biomass pretreatment and recalcitrance.

1. Introduction

With increasing energy demand, depletion of fossil fuels as well as concerns over climate change, the utilization of renewable biomass feedstock for the production of fuels, chemicals and materials has become a global research focus.^{1, 2} Based on Biomass Research and Development Act of 2000 of US Congress, the term biomass is defined as “any organic matter that is available on a renewable or recurring basis (excluding old growth timber), including dedicated energy crops and trees, agricultural food and feed crop residues, aquatic plants, wood and wood residues, animal wastes, and other waste materials.” A biorefinery is similar to that of a petrorefinery except instead of crude oil, biomass is the starting material. The concept of biomass refining was proposed in 1982.³ The US Department of Energy, in its Energy, Environmental, and Economics (E3) handbook, uses the following definition: “a biorefinery is an overall concept of a processing plant where biomass feedstocks are converted and extracted into a spectrum of valuable products, based on the petrochemical refinery” (<http://www.oit.doe.gov/e3handbook>). A biorefinery can maximize the value derived from a variety of different biomass feedstocks by producing multiple products. A similar definition can be found from the National Renewable Energy Laboratory’s (NREL’s) website: “a biorefinery is a facility that integrates biomass conversion processes and equipment to produce fuels, power, and chemicals from biomass” (<http://www.nrel.gov/biomass/biorefinery.html>).

Lignocellulosic biomass is of particular interest as a renewable and sustainable source of providing precursors and sugars for conversion into renewable fuels and chemicals.⁴ Lignocellulose generally consists of 40-50% cellulose, 25-30% hemicelluloses and 15-20% lignin and other extractable components.¹ Cellulose is a linear polymer of glucose linked together by β -(1 \rightarrow 4) glycosidic bonds whereas hemicelluloses is a branched heteropolymer of D-xylose, L-arabinose, D-mannose, D-glucose, D-galactose and D-glucuronic acid.⁵ Lignin is a random copolymer of three different phenylpropane monomer units, namely sinapyl alcohol, coniferyl alcohol and *para*-coumaryl alcohol.⁶

The effective utilization of all three components would play a significant role in economic viability of lignocellulosic biomass refinery.⁷ In general two different routes can be taken to convert biomass to value-added products: biochemical and thermochemical approaches.¹ Processes combining both the thermochemical and the biochemical approaches are also under investigation, such as syngas fermentation.⁸

Production of liquid fuels from biomass via the biochemical conversion processes typically involves several steps (Figure 1): 1) pretreatment of biomass; 2) enzymatic conversion of pretreated biomass into fermentable sugars; 3) fermentation of hexoses and pentoses into biofuels. Process integration reduces capital cost. Different strategies such as simultaneous saccharification and fermentation are being developed to lower the overall production cost.⁹ However, enzyme access to the surface of the polysaccharides is limited because polysaccharides are encapsulated via a tight covalent and hydrogen bonds to the lignin matrix.¹⁰

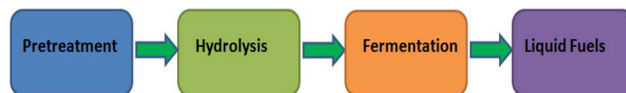


Figure 1 Biochemical Conversion of Lignocellulosic Biomass

Efficient deconstruction of lignocellulose into fermentable sugars is one of the key steps in the biological conversion of biomass to fuels. There are several challenges that must be overcome: 1) lignocellulose is a complex material which exhibits biomass recalcitrance on different length scales, that requires significant energy inputs to convert it into fermentable sugar;¹¹ 2) hierarchical structure of cellulose chains (from crystalline microfibrils to microfibrils and fibres) makes them difficult to hydrolyze,^{12, 13} and the enzymes required to do so are currently expensive to produce;¹⁴ 3) the presence of lignin occludes accessibility to polysaccharides and lignin can irreversibly absorb enzymes;¹⁵ and 4) biomass pretreatment can produce inhibitory compounds that are toxic to fuel-producing organisms.¹²

Pretreatment is a necessary step in converting lignocellulosic biomass into renewable fuels via a biochemical approach.¹⁶ It also enhances biogas production from lignocellulosic biomass via the anaerobic digestion process.¹⁷ In addition, a number of interesting studies have shown promise in upgrading bio-oil produced via pyrolysis after physico-chemical pretreatment of biomass.¹⁸ The major purpose of biomass pretreatment is to open up the compact structure of plant cell walls and increase the accessibility of cellulose.¹³ Different pretreatment technologies have been developed over the years including physical, chemical, physio-chemical and biological pretreatment.¹⁹ Typical pretreatment processes include alkaline, acid, ionic liquid, steam explosion, ammonia fibre expansion (AFEX) pretreatment, etc. Several extensive review articles of biomass pretreatment were published this year.^{16, 17, 20} Pretreatment processes often involve redistribution and removal of biomass components, with an improved surface area.¹⁹ However, degradation of biomass components also occurs during some pretreatment processes, which is an unwanted side effect because those degraded products are usually inhibitors to enzymes and microbes.¹² The selection of a pretreatment technology depends on a number of factors: the characteristics of feedstocks, the compatibility of the process with enzymes, the composition of the hydrolysates and the choices of fermentation strategies, its economic assessment and environmental impact. There has been considerable advancement in pretreatment technology and several approaches are already implemented in pilot or commercial plants for cellulosic ethanol production.²¹

Despite its critical importance in development of biomass conversion technologies, impacts of pretreatment processes on biomass recalcitrance are still not fully understood, and suitable pretreatment technologies have not been developed due to the complex interactions between plant cell wall and biomass pretreatment.²² The interactions between plant cell walls and the different pretreatment processes determine their compositional changes and structural reorganization on different length scales (Figure 2), which ultimately affect the extent of enzymatic hydrolysis.²³

Identifying recalcitrant structures in biomass has been attempted by comparing the changes in chemical compositions and physical structures during pretreatment processes and their correlations with the enzymatic hydrolysis of pretreated biomass. To date there lacks a clear picture about what plant features most strongly limit efficient enzymatic hydrolysis before and after pretreatment^{15, 24} It is generally accepted that lignin content is negatively correlated with biomass digestibility.²⁵⁻²⁷ The presence of lignin in plant cell walls physically impedes the accessibility of cellulase to cellulose and the available functional groups such as phenolic hydroxyl and aliphatic groups can irreversibly bind to cellulases.²⁵ Synthetic biology tools were used to rewire the secondary cell wall network in *Arabidopsis* by changing promoter-coding sequence associations.²⁸ Yang et al. reported a reduction in lignin and an increase in polysaccharide depositions in the plant's fiber cells, resulting in higher sugar yields after enzymatic hydrolysis.²⁸ However, Voelker et al. reported that the sugar yields of pretreated transgenic poplar wood did not increase despite the decreased lignin content.²⁹ They argued that normal wood with lignin removed during pretreatment may provide better structural access for enzymatic degradation of cellulose than transgenic wood with inherently less lignin.²⁹ Recently, glycome profiling technique was used to monitor structural changes in hydrothermally-pretreated *Populus* biomass.³⁰ DeMartini et al utilized glycan-directed monoclonal antibodies to yield a more complete depiction of alterations occurring in most major classes of plant polysaccharides during hydrothermal pretreatment.³⁰ The study suggested that the lignin content alone does not affect recalcitrance; but that the integration and association of lignin and polysaccharides within the cell wall play a more critical role in biomass recalcitrance.³⁰ These investigations emphasize the necessity of studying the plant cell wall as an integrated system of cellulose, hemicellulose and lignin as alteration of one of them generates changes in the other two.

A deeper understanding of biomass recalcitrance requires generation of better cell wall models through continuous investigations of cell wall biophysics and biosynthesis.³¹ A plant cell wall is typically deposited in three layers, namely primary cell wall, secondary cell wall and middle lamella.²⁵ Cellulose, hemicelluloses and lignin have different distributions in these layers. Not all types of cells have secondary cell walls.²³ The secondary cell wall is the predominant structure in woody biomass, which usually consists of three sub layers, S1, S2 and S3.²¹ The integrated structure of cellulose, hemicelluloses and lignin in plant cell walls is still not fully understood.³² It was proposed that ferulic acid forms covalent ester-ether bridge between polysaccharides and lignin molecules.³³ Ferulated hemicelluloses are considered as potential sites for covalent cross linking between carbohydrates and lignin, results in formation of lignin-carbohydrate complexes (LCCs).³³ A computer simulation work showed that hemicellulose branches of arabinose, glucuronic acid and glucuronate strengthen the primary cell wall by strongly coordinating to hydrogen bond donor sites on the cellulose surface.³² Differences in cell wall composition and their associations influence which component has the largest impact on the biomass recalcitrance. In an extended study by DeMartini et al., lignin and hemicelluloses were found to influence the

enzymatic digestibility of both poplar and switchgrass, but to a different degree.²⁴ While lignin content played an important role in biomass recalcitrance in poplar, the removal of hemicelluloses, specifically xylan, resulted in a larger increase in the final glucose yield than removal of lignin in switchgrass.²³ Their study suggests that different pretreatment techniques need to be considered to efficiently convert a specific biomass feedstock into sugars.

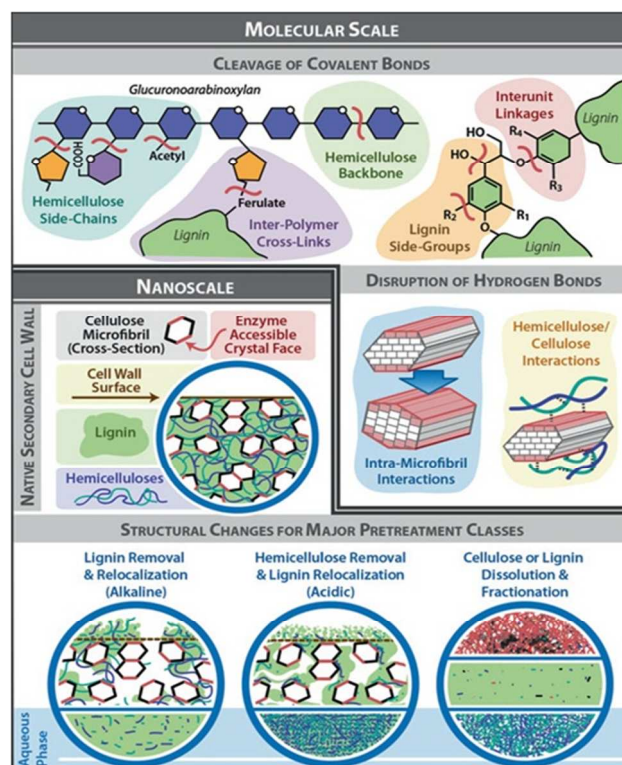


Figure 2 The interactions between pretreatment and plant cell walls generate structural changes over many length scales²³

The interactions between plant cell walls and pretreatment generates recalcitrance-related changes of physical structures on nano/micrometer length scales. Structural features such as specific surface area, porosity and cellulose crystallinity have often been investigated to gain understanding of the mechanisms of biomass pretreatment and biomass recalcitrance.^{11, 25} Recent research developments in biomass characterization reflect the importance of the multi-scale nature of the interactions between biomass pretreatment and biomass recalcitrance.³⁴⁻³⁹ There are two relatively less studied aspects that are also important to comprehend biomass deconstruction: integrity of cellulose microfibrils and redistribution of cell wall components. A multiple scale visualization and characterization of cell walls in corn stover was carried out with the help of several microscopic tools to understand nano/micrometer structural changes during ammonia fiber expansion (AFEX) pretreatment process.³⁹ AFEX pretreated cell wall surfaces were found to be non-uniformly covered by irregularly shaped, hydrophilic deposits (20–1000 nm in width).³⁹ Chundawat et al. proposed that AFEX redeposits cell wall decomposition products (e.g., amides, arabinoxylan oligomers, lignin-based phenolics) on outer cell wall surfaces.³⁹ The process of extraction leads to creation of nano-porous tunnel-

like networks throughout the cell wall. Therefore the digestibility of plant cell wall was improved without significant alterations in crystalline cellulose and biomass composition. Relocation of lignin fragments were also observed during dilute acid pretreatment in several earlier studies.⁴⁰ Donohoe et al. reported that melting of lignin during DA pretreatment caused them to coalesce into larger molten bodies that migrate within and out of the cell wall and can redeposit on the surface of corn stover cell walls.⁴¹ The size of these droplets ranged from 5nm to 10mm in diameter. It was argued that lignin re-localization opened up the structure of the cell wall and improved the accessibility of the majority of cellulose microfibrils.⁴¹ However, other researcher argued that re-deposited lignin droplets in the pretreated substrates are not desired due to their inhibitions on enzymatic hydrolysis.¹⁵ Nevertheless, these studies clearly show that lignin content itself is not enough to explain impact and efficiency of pretreatment.

The role of cellulose crystallinity has been discussed in several recent reviews and will not be detailed here.^{15, 25} In addition to cellulose crystallinity, due attention needs to be given to the size, orientation and organization of cellulose microfibrils in plant cell wall.⁴² An AFM study supports the model that a microfibril in plant cell walls of corn stover consists of 36 glucan chains.³⁴ Cellulose microfibrils have a typical dimension of 2 to 4 nm in diameters and the length of several micrometers.⁴³⁻⁴⁵ The microfibrils surrounded by glucomannan may further aggregate into bundles with diameters of tens of nanometres, and they are embedded in a lignin-carbohydrate complex.⁴⁶ Ding et al demonstrated that maintaining the integrity of cellulose microfibrillar architecture is important as the enzymatic digestion is primarily facilitated by enabling enzymes access to the hydrophobic cellulose crystalline surface.³⁴ They further suggested that ideal pretreatment should maximize lignin removal and minimize polysaccharide modification.³⁴ More recently, Inouye et al. pointed out that biomass pretreatment should maximize generation of fragments and minimize preservation of intact cellulosic fibrils.³⁶ They studied impact of dilute acid pretreatment on the micro- to nanoscale architecture of corn stover cell walls using wide angle x-ray scattering (WAXS, also known as XRD), small angle x-ray scattering (SAXS) and Ultra small angle x-ray scattering (USAXS).³⁶ The combination of these x-ray scattering techniques covers length scales from 0.22 to 500nm. It was discovered that yields from enzymatic digestion are largely due to hydrolysis of individual cellulose chains and fragments generated during pretreatment.³⁶

It becomes clear that a multiple length scale characterization of pretreated biomass is a useful strategy to identify the mechanisms of overcoming biomass recalcitrance. Imaging techniques such as electron microscopy, Raman micro spectroscopy and fluorescence microscopy have proven to be valuable tools in understanding the biomass deconstruction processes.^{11, 47} Singh et al. demonstrated that lignin dissolution resulted in cell wall swelling followed with complete solubilization of plant cell wall during ionic liquid pretreatment (Figure 3).^{37, 47} NMR is another important technique which has been used successfully in characterizing biomass components and understanding biomass pretreatment.^{48, 49} Scattering techniques including x-ray and neutron scattering, which are complementary tools, offer several

advantages like minimum sample preparation, versatile sample environment, in situ dynamic investigation of cell wall structures.^{35, 36, 38, 50-55} Among them, small angle scattering (SAS) are underutilized for biomass characterization partly due to unfamiliarity outside the scattering community and relative complexity of data analysis. In this context, WAS includes WAXS and wide angle neutron scattering (WANS). SAS includes SAXS and small angle neutron scattering (SANS). WAS measures structures of sizes on the order of 0.1nm, SAS measures structures on the order of 1nm to 100 nm. In addition, USAXS and USANS extend the length scales measured to 1000 nm. There has been an increasingly number of publications over the past two years, which took advantage of SAXS and SANS to understand structural changes during pretreatment of biomass samples.^{35, 36, 38, 50-54} The impacts of pretreatment on surface roughness of biomass, integrity of cellulose microfibrils, phase separation between cellulose, hemicellulose and lignin, relocation of lignin have been investigated. The results of these studies are encouraging in that unique information such as biomass roughness, size of microfibrils, distribution and association of lignin, hemicellulose and cellulose were revealed which was not accessible by other techniques.

It is therefore necessary to provide an overview of the interactions between scattering and biomass structures with an emphasis on understanding biomass pretreatment and recalcitrance. In comparison to x-ray scattering, neutron scattering causes little or no radiation damage, and most importantly, has the ability to highlight a particular structure in biomass samples by using contrast variation. This is significant considering the complex structures of plant cell walls. Other characteristics and potential applications of neutron scattering in the field of bioenergy has been summarized in a recent review.⁵⁵ We hope that current review will further appeal more researchers to use scattering tools in their investigations in the field of biomass and bioenergy.

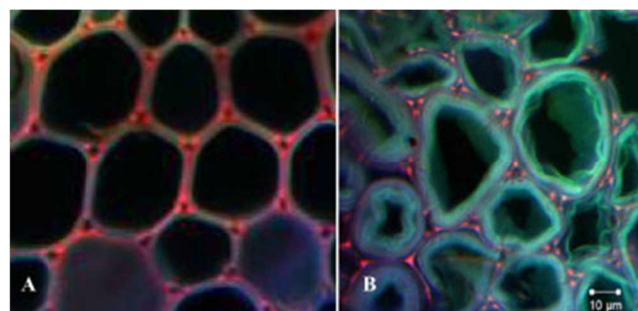


Figure 3 Confocal fluorescence images of switchgrass cell walls (a) before pretreatment and (b) swollen cell wall after 10 min pretreatment with 1-ethyl-3-methylimidazolium acetate at 120°C.⁴⁷

2. Supramolecular structure of cellulose studied by wide and small angle scattering

2.1 Wide and small angle scattering: Background

Many comprehensive discussions of x-ray and neutron scattering have been published elsewhere,⁵⁶ this section aims to give a brief introduction to the basics of SAS and WAS, a knowledge of which can help non experts in designing suitable experiments

based on research hypothesis. Mathematically speaking, both WAS and SAS present pictures in reciprocal space as Fourier transform of the scattering objects in real space. In WAS, the structure under investigation is the periodic arrangement of atoms in crystals, for example in cellulose crystallites. A crystal consists of a number of units cells arranged regularly in space with each cell having the identical atomic content. The measured scattering intensity is the absolute square of the Fourier transform of the periodic structures and it contains information about the shape of the lattice and its content. The shape of the lattice, also called the lattice factor, generates reflections under a distinct scattering angle and in a distinct direction. The relation between scattering angle and the shape of lattice can be understood in terms of the Bragg's law:

$$\sin\theta = \frac{\lambda}{d} \quad (\text{Equation 1})$$

where 2θ is the scattering angle and λ is the wavelength of x-ray or neutron beam. The distance d represents the period of repetition in the structure or the spacing between crystallographic planes. The placement of the atoms in a unit cell, also called the structure factor, determines the intensity of the scattering at distinct scattering angle and in a distinct direction.

WAXS is readily accessible at universities and research institutions and has been widely used to measure the changes in cellulose crystalline structures during biomass pretreatment. In plant cell walls, a number of cellulose chains crystallize to form cellulose microfibrils. In the crystalline regions, the cellulose chains are found to form two distinct allomorphs, I_α with a triclinic unit cell and I_β with a monoclinic unit cell, whose fractional distributions vary among samples from different origins.⁵⁷ In cellulose I, parallel chains align edge to edge via hydrogen bonding in a flat sheet and the main difference between I_α and I_β is the relative displacement of the hydrogen-bonded sheets in the chain direction.⁵⁸ A determination of the fraction of I_α or I_β is often difficult for powder samples commonly accessible in biomass conversion processes,⁵⁹ and in most of the cases the WAXS spectrum is reported to be of cellulose I.⁶⁰ The observed characteristic peaks on WAXS spectrum of cellulose I lattice varies slightly with sources of biomass, the moisture content, etc.⁵² A WAXS spectrum of cellulose I measured with Avicel (PH101) using an x-ray wavelength of 0.154nm is shown in Figure 4 as the black curve. Cellulose II is most often obtained from cellulose I via either of two processes: regeneration and mercerization.⁶¹ In the cellulose II form, chains with opposite polarity are stacked to form corrugated sheets.⁶² Hydrogen bonding exists within the sheets as well as between them.⁶² A WAXS spectrum of cellulose II measured with regenerated Avicel (PH101) from an ionic liquid solution is shown in Figure 4 as the red curve. The allomorph of cellulose and crystallinity are often measured to evaluate the influences of biomass pretreatment on biomass samples, and to correlate them with variations in enzymatic hydrolysis.^{15, 25, 63}

WAXS has been used to measure the orientation of the cellulose microfibrils in plant cells by analyzing the angular intensity distribution of reflection 004 and 200, as will be introduced in Section 2.2. The cross-section diameter of the cellulose microfibrils can be estimated by measuring the peak width of the reflection 004, assuming the contribution of lattice

distortion to the broadening of the peak is less significant. An example of utilization of this method will be presented in Section 2.3.

In contrast to WAS, the technique of SAS is used to study structures of size on the order of 1 to over 100nm. The relation between scattering angle and size of the structures measured can be also understood in terms of the Bragg's law. The distance d , size of the structures, is inversely proportional to the scattering angle 2θ . For example, when $\lambda = 0.154$ nm, $d=10$ nm, the scattering peak will appear at $2\theta=0.88^\circ$; for $d=0.1$ nm, the scattering peak will appear at $2\theta=100^\circ$. Roughly speaking, small angle scattering refers to the scattering angle $2\theta < 5^\circ$. SAS detects the structure on the nanometre scale only if there is a sufficient contrast between the structure and the surrounding media. The measured SAS intensity is the absolute square of the Fourier transform of the structures and it contains information about the shape and interactions of the structures. If the measured structures have well-defined shapes, for example, a cylinder, the SAS intensity is divided into two parts, one is called the form factor, determined by the shape and size of the structures and the other part is called the structure factor, determined by the interaction between the structures.

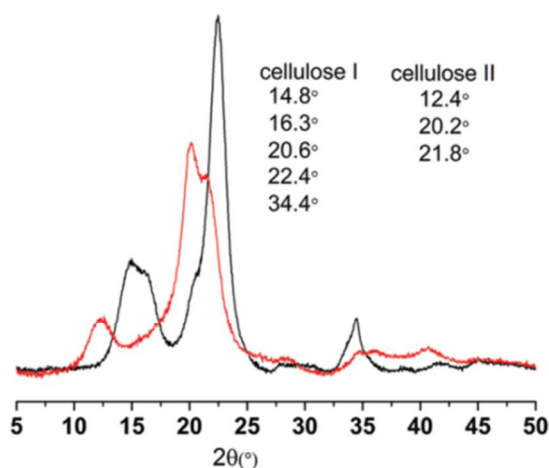


Figure 4 WAXS spectrum of Avicel and regenerated cellulose.⁶⁴

In terms of SAS, lignified cell walls are considered to consist of at least three distinct phases: cellulose microfibrils, the matrix polymer (lignin-polysaccharide complex) and voids/cracks. The SAS intensity of the radiation scattered by the plant cell wall can be written as⁶⁵

$$I(q) = I_0(\rho_{\text{biopolymer}} - \rho_{\text{matrix}})^2 \left| \int_V \exp(i\mathbf{q}\mathbf{r}) d^3 r \right|^2 \quad (\text{Equation 2})$$

Where q is the wave vector of the scattered beam and is related to the scattering angle 2θ and wavelength by $q=4\pi\sin\theta/\lambda$. The scattering contrast is given by $(\rho_{\text{biopolymer}} - \rho_{\text{matrix}})$ and ρ represents electron density in x-ray scattering experiments and the scattering length density (SLD) in neutron scattering experiments. The SLD is obtained as the sum of scattering lengths, b , for all atoms in an arbitrary volume, V , divided by the volume.⁵⁶

Plant cell walls are comprised of structures that occur over

different length scales, and the scattering may come from small pores, cross-section of cellulose microfibrils, lignin aggregates, network structures in cell wall, surfaces of cell walls or larger pores. To properly analyze the scattering data one needs to consider several factors: the relative scattering contrast between different structures, the biomass composition, possible sizes of different structures. In many cases, empirical equations that describe structural features of different sizes are used to analyze the data.^{53, 66-69}

In terms of x-ray scattering contrast, the electron density of cellulose was estimated to be 5.1×10^{23} electrons/cm³, of the matrix polymer was about 4.5×10^{23} electrons/cm³, and of water was 3.4×10^{23} electrons/cm³.⁷⁰ In terms of neutron scattering contrast, the SLD of cellulose was reported to be $1.5 - 1.9 \times 10^6 \text{ \AA}^{-2}$.⁷¹ The SLD of hemicelluloses is estimated to be $1.7 \times 10^6 \text{ \AA}^{-2}$ by assuming a chemical formula of $(\text{C}_5\text{H}_8\text{O}_4)_m$ ¹⁹ and a mass density of 1.4 g/cm^3 .⁷² The SLD of lignin is estimated to be $1.7 - 1.9 \times 10^6 \text{ \AA}^{-2}$ by assuming a chemical formula of $[\text{C}_9\text{H}_{10}\text{O}_3(\text{OCH}_3)_{0.9-1.7}]_m$ ¹⁹ and a mass density of 1.5 g/cm^3 .⁷² The neutron and x-ray scattering contrast among different components in lignocellulosic biomass samples is small. As will be shown later, the contrast in a neutron scattering experiment may be enhanced by deuteration of a particular component.

Despite the weak scattering contrast that exists between cellulose microfibrils and the polymer matrix, SAXS has been used to obtain size and orientation of cellulose microfibrils.^{44, 45, 73, 74} If we assume that cellulose microfibrils are thin, elongated cylinders, they will become flat disks (Fourier transform of a cylinder) in reciprocal space orientated perpendicular to the microfibrils.⁶⁵ The size of the disk is approximately $1/L$ in thickness and $1/2R$ in diameter, where L is the length of the microfibrils and R is the cross-section radius of the microfibrils.⁶⁵

The plant cell wall of lignocellulosic biomass contains many pores with various sizes and therefore it can be regarded as a porous material. The scattering from nano/micrometer pores in biomass samples can dominate the whole spectrum since the electron density or SLD of air is close to zero. The contrast between solid biomass skeleton and air is larger than that between different biopolymers. The interferences from pores scattering therefore complicate the data analysis, and this will be discussed using a few examples. Scattering from porous structures is typically characterized by power-law dependent scattering, which can be analyzed by two different approaches.⁷⁵

In the first approach, the power-law scattering is considered as a result of scattering from the interface of the pores, where the exponent of the power-law, α , is related to the surface fractal dimension, D_{surface} , of the surface of the pores by $D_{\text{surface}} = 6 - \alpha$. A smooth surface corresponds to $D_{\text{surface}} = 2$, while a rough surface leads to a value smaller than 2. In the case of a smooth surface, specific surface area, S , can be obtained by the Porod law. For an ideal two-phase system (having a sharp interface), Porod's law predicts that $I(q)$ decreases as $\sim q^{-4}$ for large q .⁷⁶ The proportionality constant, B , is related to specific surface area, S , and $I(q)$ by⁷⁶

$$I(q) = \frac{2\pi(\Delta\rho)^2 S}{q^4} = \frac{B}{q^4} \quad (\text{Equation 3})$$

Where $\Delta\rho$ is the scattering contrast. $I(q)$ is on an absolute scale. This method can be applied to any two-phase system with a smooth interface. The porosity, ϕ , is related to the scattering invariant Q which is calculated by⁷⁶

$$Q = \int q^2 I(q) dq = 2\pi^2 (\Delta\rho)^2 \phi (1 - \phi) \quad (\text{Equation 4})$$

The evaluation of the invariant Q often requires a combination of SAS and USAS to cover a wide q range. Another parameter of interest is the Porod length, a mean chord length characterizing the average size of the heterogeneities in a two-phase system.⁵⁶ A chord is defined as a segment that belongs either to the pore or to the solid and has both ends on the interface. The Porod length is given by:

$$l_p = \frac{4\phi(1-\phi)}{S} \quad (\text{Equation 5})$$

In the second approach, the power-law dependent scattering is explained as scattering from polydisperse pores with a pore size distribution of a power law.⁷⁵ The pore size distribution is obtained from the fit of polydisperse spherical particle model.⁷⁷

The porosity and specific surface can be calculated by the total pore volume and pore surface divided by the sample volume, respectively.⁷⁷ One advantage of measuring porosity using SAS is that the total porosity is obtained, that includes both open and closed pores.⁷⁷ In contrast to the traditional BET analysis⁷⁸, SAS experiments can be performed on wet samples, which is more relevant to the enzymatic conversion of biomass samples.⁵⁴

Table I provides the examples of studies of the structure of lignocellulosic biomass using scattering techniques. Although very useful, USANS and USAXS have been rarely used to study biomass structures until now, therefore they are not included in Table I. Selective references of the studies listed in Table I will be presented in detail in the following discussions. Table I is not intended to be an exhaustive summary of the literature studies, instead typical examples of biomass characterization using x-ray and neutron scattering are presented which demonstrate the capability of scattering tools. For more practical applications of SAS, readers are referred to a recent review article.⁷⁹

2.2 Measurement of Microfibril angle

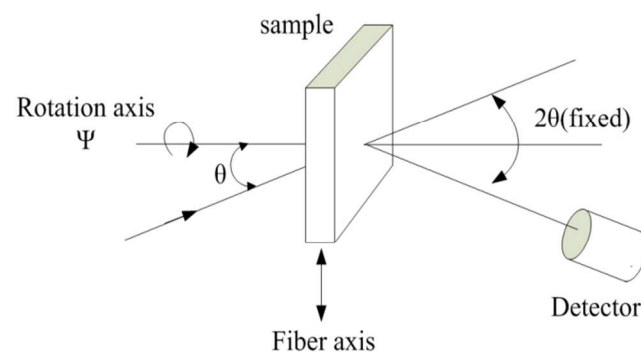


Figure 5 The symmetric transmission geometry for determination of the MFA

Microfibril angle (MFA) is the angle between the parallel cellulose chains and the fibre axis.⁸⁰ MFA is one of the properties which determine the strength of the wood cells, and it is affected by both genetic and environmental factors.⁸¹ MFA has been found to decrease with distance from the pith and becomes constant in mature wood.⁸¹ Both WAXS and SAXS have been used for determination of the MFA.^{74, 80, 82, 83}

For the MFA measurement in a symmetric transmission mode (Figure 5), a one dimensional detector is fixed to the reflection position. The sample is rotated around its normal axis and the

intensity is measured as a function of the angle, ψ . The WAXS experiments for determining the distribution of MFAs has been done using both the reflections 004 and 200 to obtain information on the MFA and shape of the cell cross-section.^{80, 82} When the cells are rectangular, the azimuthal intensity profiles of the 200 and 004 reflections have the same shape. When the reflection 004 is used for data analysis, its azimuthal intensity distribution is given by four diffraction spots with their positions related to the MFA (μ) via $\psi=90^\circ\pm\mu$ and $270^\circ\pm\mu$. When using reflection 200,

Table 1 Examples of lignocellulosic biomass characterization using x-ray and neutron scattering

Structures of interest	Information acquired	XRD	SAXS	SANS	x-ray and neutron reflectivity	Details of data analysis with references
Cellulose crystallinity		√				peak height; peak deconvolution; amorphous subtraction ⁶⁰
Cellulose microfibrils	Diameter		√	√		Fitting the SAXS or SANS data to form factors of long cylinders with rectangular, circular or elliptical cross-section ^{44, 45, 72, 84}
	length of crystallite along the microfibrils	√		√		peak width of reflection 004 in XRD; ^{45, 85, 86} using the Bragg equation in SANS ^{87, 88}
	width of crystallite perpendicular to the microfibrils (on the same order of the diameter)	√				peak width of reflections 110, 1-10 and 200 in XRD ^{45, 80, 81}
	microfibril angle	√	√			evaluation of angular intensity distribution of reflections 200 and 004; ^{65, 80-83, 89, 90} evaluation of angular SAS intensity distribution of microfibrils ^{65, 74, 91}
Pores in plant cell wall	Porosity		√	√		one approach requires calculation of the scattering invariant; ^{76, 92} another approach needs fitting the data to polydisperse spherical model ⁷⁷
	specific surface area		√	√		one approach requires application of the Porod law; ^{72, 87} another approach needs fitting the data to polydisperse spherical model ⁷⁷
	pore size distribution		√	√		fitting the data to polydisperse spherical model ^{66, 67, 77}

	surface roughness		√	√		A smooth surface corresponds to a surface fractal dimension of 2, while a rough surface leads to a value smaller than 2 ^{52, 54}
	Porod length		√	√		Needs both the specific surface area and porosity ^{70, 92}
Solution structure of extracted lignin	size, shape and association of lignin in solutions		√	√		Fitting the SAXS or SANS data to form factors of objects with different shapes ⁹³⁻⁹⁵
Aggregates of microfibrils or lignin in cell walls	Aggregation or phase separation occurs as a result of pretreatment	√	√	√		analysis of the data were performed qualitatively ^{38, 50, 51} or semi-quantitatively ⁹²
Hierarchical structures of cellulose or plant cell wall	scattering from pores, cross-section of cellulose microfibrils, lignin aggregates, network structure in cell wall, surfaces of cell wall or pores		√	√		Empirical equations are often used which describes structural features with different sizes ^{53, 66-69}
Smooth cellulose film	enzymatic digestion of cellulose films				√	Extracting volume fraction of cellulose in the direction perpendicular to the film surface ^{71, 96, 97}

there are also four diffraction spots with their positions related to the MFA by $\psi = \pm\mu$ and $180 \pm \mu$. The derivation of MFA using reflection 004 is independent of the cells' shape while for the analysis of the data using reflection 200, the knowledge of the cross-sectional shape of the cells is required. In the case of cells with a round cross-section, the azimuthal intensity profile of the 200 reaches a maximum at $\psi = \pm \arcsin(\sin\mu/\cos\theta)$.⁶⁵ Theoretically, the MFA distribution can be measured directly using the reflection 004, but in practice the intensity distribution is contaminated by scattering intensity from nearby lattice planes.⁸² The reflection 200 is free of contaminations from other lattice planes; however its intensity distribution contains information on both the MFA and the shape of the cross-section.⁸²

In one study, the MFA of tracheids in Sitka Spruce from four provenances were measured by WAXS.⁹⁰ In part of the samples, the intensity curve for reflection 004 consisted of two, well separated peaks and the curve for reflection 200 was broad and had its maximum at zero angle. This indicates that the cell cross-section is not rectangular.⁹⁰ For comparison, the intensity curve in Figure 6 for reflection 004 was shifted by 90°. In that study, the intensity curve for reflection 004 was used to obtain the MFA. The MFA was interpreted as arising from the S2 layer. In the data analysis, the MFA distribution was presented as a sum of two or three pairs of Gaussian functions. For the sample shown in Figure 6, the MFA equals to 23° with a standard deviation of 9°. The MFA arising from the S1 or S3 layer often occurs at higher angles

and their scattering intensity is lower due to their lower content in the cells.⁹⁰ For an example of determining the MFAs from S1, S2 and S3 simultaneously, the readers are referred to Serimaa.⁸⁹

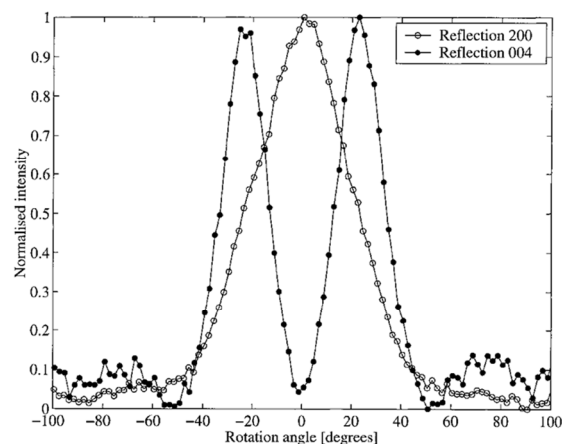


Figure 6 The azimuthal intensity curves for reflections of 200 and 004 of a Sitka Spruce sample.⁹⁰

For anisotropic SAS, the scattering intensity, $I(q)$ is expressed as $I(q, \psi)$, where ψ is the azimuthal angle of q in the detector plane. A schematic of SAS configuration is shown in Figure 7. The integral in equation 2 yields information on shape, size and

orientation of the cellulose microfibrils.⁹⁸ The MFA can be extracted from the angular distribution of the scattered intensity⁹⁸

$$I(\psi) = \int_{q_1}^{q_2} I(q, \psi) dq \quad (\text{Equation 6})$$

The scattered intensity obtained from the experiment was therefore integrated over q and plotted versus the azimuthal angle ψ . The resultant curve is then evaluated to obtain the MFA. For the cells with a square cross-section, there is a superposition of four streaks at angles ψ given by

$$\tan \psi = -\tan \mu \cdot \cos \alpha \quad (\text{Equation 7})$$

where $\alpha = \omega + n\pi/2$ ($n=0,1,2,3$), corresponding to the four sides of the square.⁶⁵ ω is the rotation angle of the sample around the

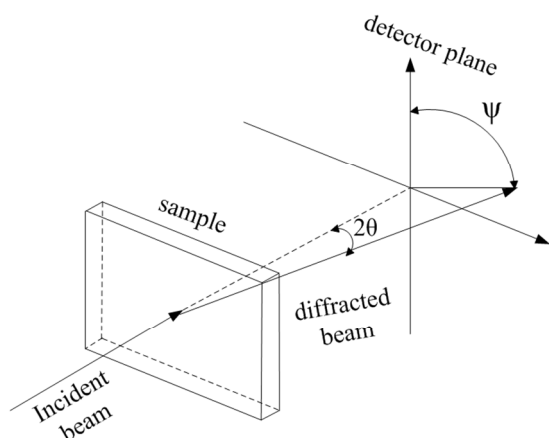


Figure 7 SAS geometry for determination of the MFA

tracheid axis, which is equal to 0 when the square is positioned at right angles to the incoming beam. In that case, as presented in Figure 8, two streaks coincide at $\psi = 0$, two streaks appear at $\psi = \pm\mu$.^{10, 74} If the cells have a circular shape, the intensity distribution becomes independent of the rotation angle and is strongly peaked at $\pm\mu$.⁶⁵

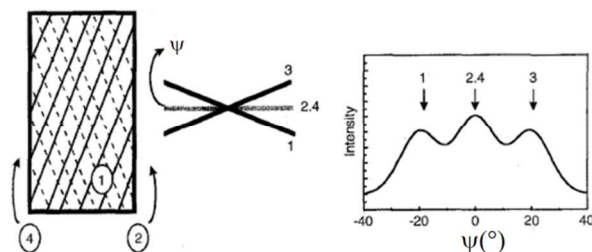


Figure 8 Rotation dependence of the measured MFA with rectangular cross-section. Four streaks are expected with two of them superimposing for a rotation angle of zero.⁷⁴

An example of measuring MFA in a spruce branch by SAXS is shown in Figure 9.⁹¹ The curve was fitted with three Gaussians

of equal width. In case of rectangular cells, the microfibril angle μ is given by the distance of the outer peaks. A map of MFA all over the branch was obtained as a function of the distance from the trunk within each annual ring. It was found that in compression wood the MFA decreased continuously from the trunk towards the tip in all annual rings.⁹¹

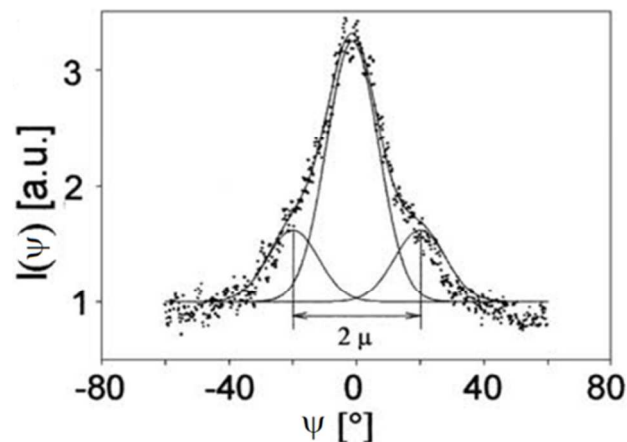


Figure 9 The scattered intensity was integrated over the scattering vector q and plotted versus the azimuth angle ψ .⁹¹

2.3 Measurement of cellulose microfibrils diameters by scattering techniques

Accurate evaluation of the diameter of cellulose microfibrils requires knowledge of cross-sectional shape of microfibrils. Cellulose is extruded from terminal enzyme complexes (TC) located in the cell wall.⁹⁹ The configuration of the TCs dictates the resulting microfibril architecture. For trees and plants, the TC is believed to be organized into six-membered rosettes with each subunit producing a linear sheet of 6 cellulose chains.¹⁰⁰ From a single TC the resulting cellulose elementary fibril has 36 cellulose chains, and a square cross-section with (110) and (1 $\bar{1}$ 0) terminating surfaces.¹⁰¹ This model is consistent with WAXS analysis of wood cellulose nanocrystals (CNCs) prepared by acid hydrolysis.¹⁰² The average lateral dimensions of the microfibrils can be calculated from (200), (1 $\bar{1}$ 0) and (110) crystallographic planes by measuring the full widths at half heights, assuming that the finite size of crystallites dominate broadening of the x-ray reflections.^{45, 102} Based on AFM measurements, a 36-chain diamond-shaped model was proposed for cellulose microfibrils in corn stover stem.³⁴ A diamond-shaped cross-section was also presented in a study of cotton cellulose nanowiskers by WAXS and NMR; however each microfibrils contained more than 36 chains.⁸⁶ Alternatively, a 24-chain model with a rectangular cross-section was the preferred choice for microfibrils in spruce wood based on SANS and WAXS data.¹⁰³

The scattering from crystallite region has been modelled as infinitely long, uncorrelated cylinders, where the SAXS data were fitted with the form factor

$$P(q) \propto J_1(qr)^2 / qr^2 \quad (\text{Equation 8})$$

where J_1 is the Bessel function of the first kind and r is the radius

of the cylinder.⁴⁵ The length of the crystallites was usually outside the measurement range of typical SAXS experiments, in addition to the possible interferences from scattering of larger pores. When the microfibrils are closely packed in space, an interference function needs to be included in the data analysis.⁴⁵ Equation 8 was used to analyze SAS data from Norway Spruce, the extracted diameter of microfibrils was 3 nm and agreed well with that obtained from WAXS data⁸³. Distinct peaks arising from packing of cellulose microfibrils were observed in SAXS data of celery collenchymas and spruce cell walls.⁴⁴ A model of non-interacting disks convoluted with a modified Lennar-Jones energy potential was used to produce liquid like molecular packing. The data analysis revealed that microfibril diameters were not uniquely determined, and in the range of 2.4 to 3.2 nm, the model reproduced the SAXS data equally well with adjustable packing density. A mean center-to-center distance of 3.6nm, derived from the inference peak on the SAXS patterns, suggested that there were gaps between adjacent microfibrils. The gaps presumably contained hemicellulose chains that were packed loosely enough to provide x-ray contrast with the microfibrils.⁴⁴

SAXS analysis of cellulose in various wood species, cotton and flax was performed where microfibrils were modelled as infinitely long cylinders with rectangular, circular or elliptical cross-section with or without a size distribution.⁴⁵ The data in the q range of 0.095 to 0.35 Å⁻¹ was used for the analysis. For spruce wood samples, a two-dimensional paracrystal model was used as the interference function; and the mean distances between the microfibrils and the mean diameters of the cross-sections of the microfibrils were used as fitting parameters. For other samples, the SAXS data did not show interference peaks, therefore only the form factors were applied to the data analysis. The lateral dimensions of the microfibrils varied from 2.5 to 3.8 nm. A rather large cross-section was found for microfibrils in cotton linter, which had a rectangular cross-section with a dimension of 7.0×4.0 nm.⁴⁵ In order to explain the smaller sizes of the diameters extracted from SAXS data than those from WAXS data, Leppänen et al. argued that microfibrils contain a crystalline core covered with one layer of less ordered cellulose chains.⁴⁵ SAXS detects the crystalline core of the microfibril and WAXS is the most sensitive for the large well-ordered crystallites.⁴⁵ The presence of one layer of less ordered chains has been the basis of estimating the diameters of cellulose microfibrils by NMR.^{86, 104} By comparing the contributions from chains buried within the crystallites and chains exposed at the surface, the fraction of the interior chains is estimated and it is related to the diameter of the microfibrils based on a square cross-sectional model.⁸⁶ A WAXS study on the structure of microfibrils in primary cell walls from collenchyma indicates that most of the chains accessible to deuteration were located at the microfibrils surfaces rather than in amorphous domains.¹⁰⁵ Models taking into account of spatial distribution of cellulose morphologies within a cellulose microfibril, and accessible and inaccessible microfibril surfaces within microfibril aggregates have been proposed, as shown in Figure 10.^{48, 106}

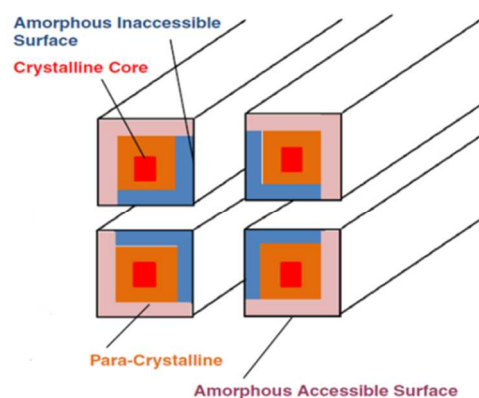


Figure 10 Schematic of a cellulose aggregate^{48, 106}

2.4 Alternating crystalline and amorphous domains in microfibrils

In addition to being present on surfaces, amorphous cellulose is often considered to be embedded within cellulose fibres. The periodic structure (Figure 11) along cellulose fibre direction is usually observed for higher plant, while bacterial and algal cellulose may not possess such structures.¹⁰⁷ The length of the crystallites along the fibre directions in principle can be estimated from (004) reflections.⁴⁵ However, it was pointed out that defect such as twisting of the microfibril contributed to the loss of axial coherence.¹⁰³ Direct measurement of structure of alternating disordered domains and crystalline regions by SAS has been rarely reported. Since the x-ray scattering density contrast between crystalline and disordered regions in cellulose is small; the periodic arrangement is usually not measurable by SAXS. The scattering contrast can be enhanced in SANS experiment by deuterium exchange of labile hydrogen atoms in disordered water accessible regions with heavy water. In the crystalline domains chains are tightly packed together which prohibit water penetration within the experimental time scale. In an early study, longitudinal periodic structures were observed for regenerated Fortisan and Rayon cellulose, with a length scale of 15 to 20 nm.⁸⁷ However, native Ramie fiber did not exhibit characteristic peaks indicating a longitudinal periodic structure. It was speculated that either Ramie cellulose did not have such a structure or the scattering from void concealed the signals.⁸⁷ Later, a meridional Bragg reflection, corresponding to a longitudinal period of 150 nm was observed in native Ramie.⁸⁸ The disordered regions consisted of 4 to 5 glucose residues. The meridional scattering was observed only after subtracting of SANS data of regular Ramie from deuterium-exchanged Ramie.⁸⁸

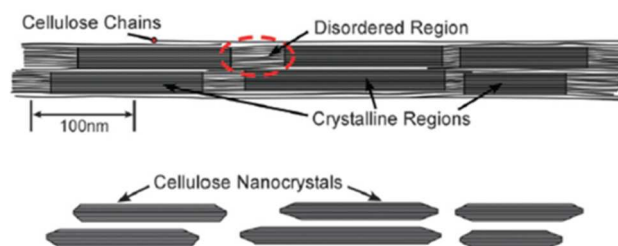


Figure 11 Schematic of periodic structure along cellulose fibres and cellulose nanocrystals.¹⁰¹

The main support for the structure of alternating crystalline and amorphous domains in microfibrils comes from isolation of cellulose nanocrystals (CNCs) via acid hydrolysis. Disordered or paracrystalline regions of cellulose are preferentially hydrolyzed, whereas crystalline regions that have a higher resistance to acid attack remain intact. Following an acid treatment and sonification, cellulose rodlike nanocrystals are produced (Figure 11).^{101, 107} Ideally, homogenous CNCs are prepared if the disordered domains along the cellulose microfibrils are completely removed by acid hydrolysis. However a wide distribution of the length and width of cellulose CNCs are often reported due to incomplete hydrolysis of disordered domains.¹⁰⁷ There are experimental evidences that correlate the length of rodlike nanocrystals with that of the crystal sizes along the longitudinal direction of cellulose microfibrils.⁸⁸ The size and shape of cellulose nanocrystals are usually determined by microscopy, however particle aggregation occurs during the drying of the samples for imaging measurement which complicates data interpretation.¹⁰⁷ CNC suspensions have also been studied using scattering methods, such as light scattering¹⁰⁸, SANS¹⁰⁹. In the SANS study, samples were made from tunicates after sulphuric acid treatment.¹⁰⁹ Due to the presence of sulfate groups on the surfaces of CNCs, they were able to form aqueous suspension. SANS analysis showed that that CNCs are long and rigid fibres whose cross-sectional shape is rectangular.²¹

One may expect that the CNCs possess higher values of crystallinity than those of untreated cellulose. XRD analysis of the CNCs prepared by acid hydrolysis of Avicel¹¹⁰, recycled pulp¹¹⁰, bleached rich husk cellulose¹¹¹ and filter paper¹¹² confirmed this hypothesis. On the other hand, prolonged exposure to acidic solutions led to decrease in crystallinity presumably since crystalline domains started to be hydrolyzed.^{113, 114}

There are fewer studies of preparing CNCs by enzymatic hydrolysis.¹¹⁵ Cellulases consist of endoglucanases, exoglucanases and cellobiohydrolases. They act synergistically in the hydrolysis of cellulose. Among those endoglucanases attacks randomly and preferably hydrolyzes the amorphous regions.¹⁰⁶ Several attempts have been made to prepare CNCs by biological processes.¹¹⁶⁻¹¹⁸ In one study, the enzymatic treatment of recycled pulp resulted in CNCs with widths of 30 to 80 nm and lengths of 100 nm to 1.8 μm .¹¹⁶

Similar to CNCs prepared by acid hydrolysis, a higher value of crystallinity was expected. This hypothesis has been challenged because some findings indicate that the crystallinity of cellulose does not change appreciably during enzymatic hydrolysis.^{67, 85, 119} Avicel was hydrolyzed with a mixture of commercial enzyme preparations (Celluclast 1.5L and Novozyme 188) at a loading of 20 mg protein/g glucan.⁸⁵ The CrI stayed unchanged over the course of 75 hours hydrolysis. It was concluded that enzymes, with a typical diameter of 6 nm, degrade the bundles of microfibrils from outer surface or from surfaces of outer pores, proceeding layer by layer. The more easily accessible bundles are degraded faster, with less accessible bundles can remain almost intact.⁸⁵ Enzymatic preparation of CNCs perhaps is currently less favourable in part due to fact that the mechanism of enzymatic digestion of cellulose fibres remains unsolved. In addition, enzymatic hydrolysis of cellulose fibres is usually a slow process. As cellulose fibres consist of aggregates of microfibrils (Figure

10), the enzymes need to digest from outside in.¹⁰⁶ On the other hand, small molecules like sulphuric acid however can penetrate cellulose fibres through voids or cracks more easily and this may lead to differences observed in characteristics of CNCs from acid pretreatment and enzymatic hydrolysis. More work is needed to improve enzymatic preparation of CNCs; for example, by mixing with the help of mechanical shearing to improve accessibility of amorphous domains to cellulases.¹¹⁸

3. Supramolecular structure of lignin: inferences using SAS studies

Lignin is synthesized by radical polymerization of phenylpropanoid units (monolignols), namely, coniferyl, sinapyl and p-coumaryl alcohols, which correspond to the guaiacyl(G), syringyl(S) and p-hydroxyphenyl (H) structures of lignin respectively.¹²⁰ The process of random radical polymerization explains the extensive structural diversity of natural lignin. The lignin macromolecule is primarily connected through carbon-carbon and carbon-oxygen bonds between building blocks of phenylpropane monomers. The most common and major inter-unit linkages in lignin are β -O-4, β -5, β - β , β -1 and their relative proportions are dependent on biomass sources as well as the lignin isolation processes employed.^{33, 49, 121}

Lignification occurs within a carbohydrate matrix of the middle lamella and secondary walls.⁶ Studies of structural organization of lignin in cell walls were carried out by TEM combined with the lignin skeleton method.¹²² Researchers found that lignin of the secondary cell wall has a loose network-like structure formed by globular particles bunched into aggregates of different shapes and sizes.¹²² In the central layer, the average size of these aggregates was equal to 38 nm. The lignin nanoparticles are probably scattered at first and then further associate to form lignin supramolecules.⁶ Due to a low degree of order and a high level of heterogeneity, isolation of unaltered lignin for structural and/or compositional analyses remains a challenging task, since the various physico-chemical techniques used for breaking down the walls also cause substantial alterations to lignin structure.⁶ Ball milled wood lignin and enzymatic mild acidolysis lignin are perhaps the closest to the *in vivo* native lignin.^{6, 123}

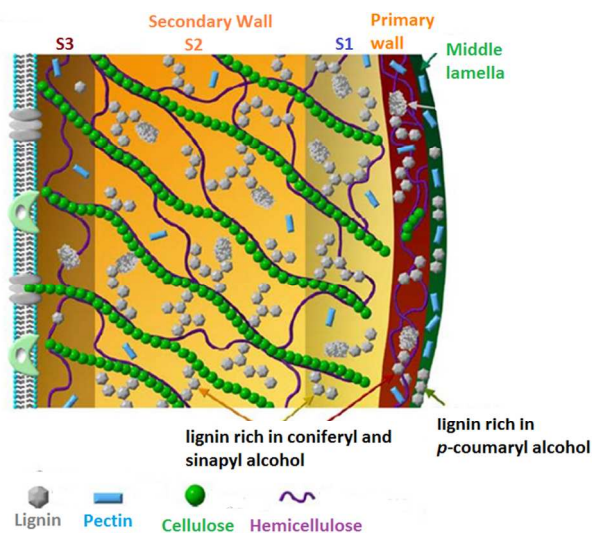
In order to mimic lignification, coniferyl alcohol was polymerized in a pectin solution.¹²⁴ Pyrene fluorescence spectroscopy showed that dehydrogenative polymer (DHP) and pectin formed hydrophobic clusters. At length scales below 30 nm segregation between pectin and DHP-rich phases were observed by SANS. Evidences provide by SANS further suggested that DHP and pectin rich phases were both dense and homogeneous as length scales above 5 nm.¹²⁴ A scanning electron microscopic study of the molecular organization of the enzymatically polymerized DHP of coniferyl alcohol on a cellulose substrate showed a globular structural unit (subunit) with a diameter of \sim 5 nm as well as aggregates of subunits.¹²⁵ The subunits correspond to individual lignin macromolecules and were connected through intermolecular forces.¹²⁵

While it is difficult to examine the lignin *in planta* by scattering or other imaging techniques, there have been a handful of studies on the solution structures of lignin. Several types of isolated lignin were studied in solution by size exclusion

chromatography (SEC) and light scattering to determine the molecular weight and size of lignin macromolecules,¹²⁶⁻¹³³ but interpretation of the data was complicated by the aggregation of lignin macromolecules.^{127, 131} SAXS and SANS are able to reveal the structures of both the aggregates and individual lignin macromolecule in solutions. SAXS studies of kraft lignin in aqueous NaCl (pH=7) and NaOH (pH=12.8) solutions showed an elongated shape with a radius of gyration between 1.6 and 3.5 nm.¹³⁴ SAXS studies of lignosulfonate particles dissolved in 0.2M NaCl aqueous solution revealed an oblate shape.⁹³

The solution structures of three types of isolated lignin - organosolv (OS), Kraft (K), and low sulfonate (LS) were studied using SANS and dynamic light scattering (DLS).⁹⁴ The results indicated that each of these lignins is comprised of aggregates of well-defined subunits. LS lignin contained a substantial amount of nanometre-scale individual subunits. In aqueous solution these subunits have a well-defined elongated shape described well by ellipsoidal and cylindrical models. Solvent-extracted lignin from a mixture of hardwood, modified with various acyl chlorides, was also studied by SAXS and SANS in tetrahydrofuran solution.⁹⁵ No association of lignin subunits was observed by SANS. Results show that individual lignin subunits have a diameter of 2 to 5 nm and they are rigid and complex, ranging from nanogels to hyperbranched macromolecules.⁹⁵

According to some researchers, the shape and size of lignin particles were determined by the shape of the spaces between cellulose microfibrils that are filled during lignifications of plant cells.¹²² A literature survey shows that the molecular weight of lignin particles extracted by various methods is in general less than 10,000g/mol.^{127, 132, 134-136} A recent NMR study on milled wood lignin and enzymatic mild acidolysis lignin, which are considered to be less modified than lignin extracted by most other methods, show that these lignin particles have an average degree of polymerization less than 10, indicating that they are oligomeric.¹²³ It is likely that there exist lignin subunits with sizes of a few nanometres in plant cell walls. These lignin subunits are hypothesized to further assemble into supramolecular structures though either polymerization or association (Figure 12).⁶

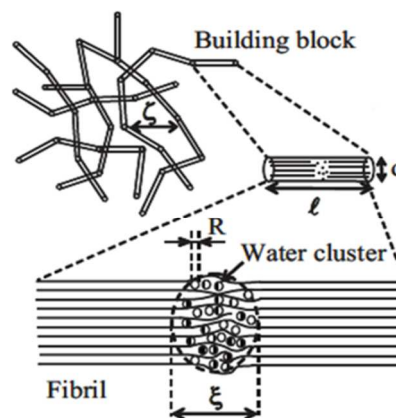


40 Figure 12 Schematic representation of association of lignin subunits in plant cell walls⁶

4. Pores in cellulose fibres and plant cell walls studied by SAS

The two-dimensional (2D) SAS patterns from aligned cellulose fibres are often diamond-shaped^{87, 88, 137-139}. In an early SANS study of native Ramie fibres, the diamond-shaped pattern was attributed to the scattering from diamond-shaped voids with a low aspect ratio.⁸⁷ That assignment was based on the assumptions that the cellulose microfibrils have a very large aspect ratio that they cannot produce diamond-shaped scattering patterns and there were no other structures that can produce significant meridional scattering. Following that, SAXS data of ramie native cellulose fibres and of regenerated Tencel[®] cellulose fibres were interpreted as scattering by a dilute phase of long thin voids, with their long axis showing a preferred orientation parallel to the fiber axis.^{137, 138} Elongated voids, approximately 2 to 30 nm wide, were shown to occur between the microfibrillar and macrofibrillar levels. The meridional broadening seen in the wet fibres was interpreted as increased misorientation of the voids and a reduction in void length.¹³⁷ On the other hand, the 2D diamond-shaped SANS patterns from scattering of ramie fibres were not interpreted as originating from pores in another study.⁸⁸ Nishiyama et al. did not find any pores on the surface of ramie fibres by TEM.⁸⁸ They argued that the periodic disorder along cellulose microfibrils caused additional meridional scattering, where the equatorial scattering was assigned to microfibrils.⁸⁸ Recently, in a study of micro-voids evolution in polypropylene during mechanical deformation, the voids were modelled as cylinders of finite length.¹⁴⁰ Diamond-shaped SAXS patterns were fit with the form factor of a cylinder with a log-normal size distribution of radius and length.¹⁴⁰

Scattering from both cellulose microfibrils and pores are often encountered in lignocellulosic biomass samples.^{44, 45, 72, 83, 84} In a SAXS study of hydration on the cell wall structure of specimens of spruce, the scattering at $q < 0.03 \text{ \AA}^{-1}$ was attributed to pores and other cavities based on the fact that the contrast between pores and the cell wall substances was reduced when the voids were filled with water.⁷² The scattering patterns in the q range of 0.05 to 0.30 \AA^{-1} were attributed to cellulose microfibrils.⁷²



80

Figure 13 Hierarchical structure of cellulose chains in papers⁶⁶

Smaller pores with their sizes concentrated around a few nanometers have also been shown to exist in papers^{66, 141}, Avicel⁶⁷ and corn stover^{54, 142}. Water clusters embedded within the network of cellulose fibres in papers were studied by SANS. De Spirito et al⁵ proposed a multi-scale complex structure of a sheet of paper (Whatman No. 1), as shown in Figure 13.⁶⁶ Small pores are intercalated between microfibrils which constitute each cylindrical segment with a length L and radius R . On a larger length scale, a cellulose network structure is formed by entangled cellulose fibres, and each cellulose fibre consists of several cylindrical segments. The SANS data of swollen cellulose fibres in papers were modelled as two parts in an empirical equation. The scattering from solvent clusters was described by a collection of spheres distributed in space with a mass fractal dimension d_f up to a distance of ξ . The scattering from the surfaces of cellulose fibres was reduced to the Porod law.

5. Enzymatic hydrolysis of cellulose monitored by SAS

The structural and morphological heterogeneity of lignocellulosic substrate hinders our understanding of mechanism of enzymatic hydrolysis of cellulose.¹⁴³ A common feature of cellulose hydrolysis is that the reaction rate decreases dramatically with the extent of conversion. Many rate limiting factors have been proposed in order to better understand the mechanism of enzymatic hydrolysis of cellulose.¹⁴⁴ In-situ monitoring of changes in physical structures, for example, cellulose crystallinity, cellulose microfibrils, microfibril networks, and porosity during conversion is essential to understand the kinetic slowdown during enzymatic hydrolysis. SAS is capable of providing dynamic information on morphological changes during enzymatic hydrolysis.

There have been several studies on the structural changes in cellulose during enzymatic hydrolysis by SAS in order to develop a better understanding of the interactions between cellulases and solid substrates. In an early study of morphological changes of cellulose (Avicel PH101) during enzymatic digestion, a distinct knee in SANS intensity was observed at $q \sim 0.1 \text{ \AA}^{-1}$ (Figure 14).⁶⁷ This was attributed to the scattering of water-filled pores within cellulose fibres. Under weak contrast conditions (30% D₂O, 70% H₂O), where the SLD is close to that of cellulose, the knee disappeared, demonstrating that water penetrates into pores throughout the entire sample.⁶⁷

A similar approach as that of De Spirito et al. was used to quantitatively analyze the data, with a different equation to describe the scattering from water clusters in cellulose fibres.⁶⁷ Water pools were modelled as spheres of radius R with a log-normal distribution of radii, $f(R)$, and distributed with a mass fractal dimension D_2 up to a cut-off dimension, ξ .⁶⁷ Kent et al. found that the extent of digestion was limited to roughly 30% in 24h for digestions performed in the absence of stirring.⁶⁷ The high q knee remained unaffected upon digestion. In presence of stirring, digestion proceeded to a much greater extent. The scattering attributed to distinct water-filled pores was rapidly lost, indicating digestion around the larger nanopores throughout the volume of the fibres.⁶⁷ The same group also used neutron reflectivity (NR) to investigate the action modes of

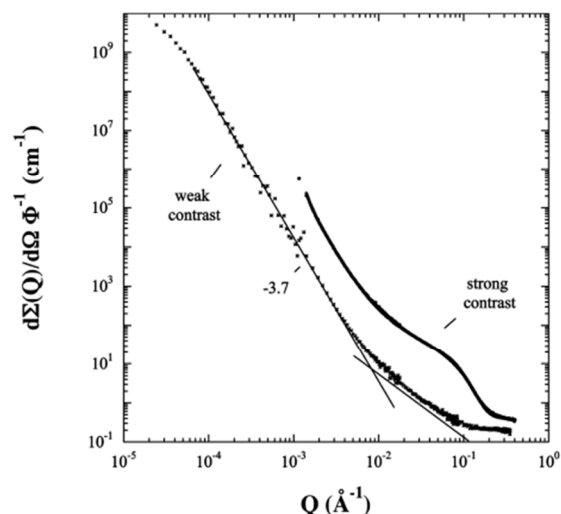


Figure 14 SANS data for ~20 wt % FD100 in weak contrast conditions (30% D₂O buffer, 70% H₂O buffer) and strong contrast conditions (100% D₂O buffer).⁶⁷

endoglucanases with and without a cellulose binding domain (CBM) on thin films of cellulose coated onto silicon substrates.^{71, 96, 97} NR presents information of the volume fraction of cellulose as a function of the distance from the interface of cellulose/substrate. Cheng et al.^{71, 96} and Reyes-Ortiz et al.⁹⁷ showed that the presence of a CBM enabled endoglucanases to penetrate and digest within the bulk of the films to a far greater extent than those without a CBM.

The high q knee on SANS pattern around $q = 0.1 \text{ \AA}^{-1}$ was also observed in a study of sub micrometer structural change during enzymatic hydrolysis of microcrystalline cellulose (Figure 15).⁸⁵ In that study, SAXS data were analyzed with a two phase model consisting of crystalline cellulose and a water matrix surrounding them. The SAXS data was not fitted with any particle form factors; instead, a chord length (the Porod length) was extracted. A chord length in a two-phase model represents average distance between interfaces. However, no definite conclusion was drawn on the effect of hydrolysis on the structure of cellulose based on the results on the chord length.⁸⁵

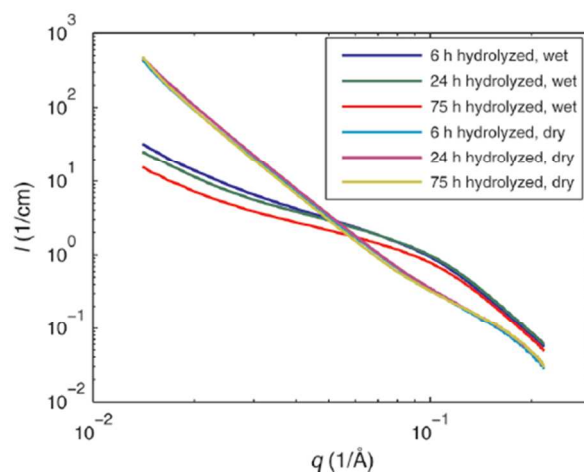


Figure 15 SAXS curves of microcrystalline cellulose hydrolyzed enzymatically for various times.⁸⁵

Birch wood chemical pulp with different xylan content were used in a SANS/SAXS study of structural changes of microfibril network during enzymatic hydrolysis.⁶⁸ The scattering data were analyzed with an empirical equation of the form:

$$I(q) = \frac{A}{q^n} + \frac{C}{1+(\xi q)^m} + B \quad (\text{Equation 9})$$

The first term describes the power law or Porod type behaviour of the scattering intensity and the second term characterizes the fibril network with a mesh size of ξ .⁶⁸ In that work, the mesh size was interpreted as the interfibrillar distance. This distance was shown to remain unchanged during digestion of the samples with high xylan content, whereas it increased in the samples with lower xylan content. The study also found that larger, recalcitrant structures remained intact after enzymatic hydrolysis.⁶⁸

More recently, SANS and SAXS techniques were applied to investigate the evolution of cellulose structure during enzymatic hydrolysis (Figure 16).¹¹⁹ Micro-crystalline cellulose and a bleached sulfite pulp were chosen as substrates. The scattering data in a q range of 0.02 to 0.3 \AA^{-1} was ascribed to that from microfibrils, instead of pores. A cylindrical form factor was however not used to fit the data. The cross-sectional radius of microfibrils was obtained from the ratio of surface to volume, calculated based on the SANS data in the low q . Chauve et al. found that the mean diameter of microfibrils in Avicel and in bleached sulfite pulp was 3.3 and 5.0 nm, respectively. The radius did not change during enzymatic hydrolysis, indicating there is no evolution in cellulose nanostructure. They proposed that enzymes degrade cellulose layer by layer, microfibril by microfibril, and enzymes cannot penetrate cellulose structure. The conclusions were partially consistent with those of prior SANS and SAXS studies, except that it did not mention the role of pores present in cellulose fibres during enzymatic digestion.^{67, 85} This is in contrast to the studies where cellulose is presented in the form of smooth amorphous thin films, and cellulases with a binding domain are able to penetrate into the films.^{71, 96, 97}

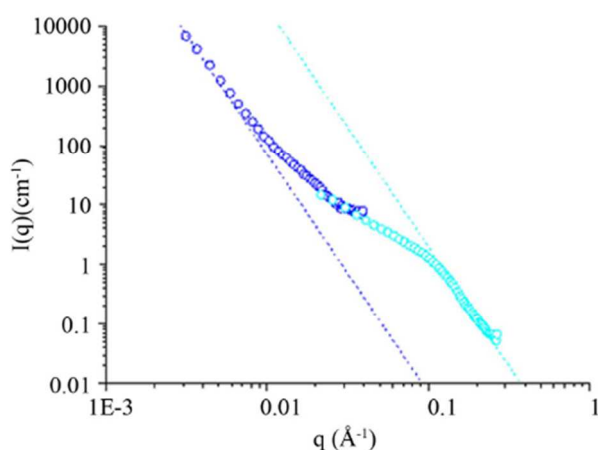


Figure 16 SANS data of hydrolyzed Avicel with 10% glucan conversion¹¹⁹

6. Understanding physical structural changes during biomass pretreatment using scattering techniques

XRD (WAXS) has been most widely used to study the changes in crystalline structure of cellulose during biomass pretreatment. More recently, a few studies reported the variations in the diameter of cellulose microfibrils, suggested by XRD data.^{38, 42, 51} Aggregation and coalescence of microfibrils during pretreatment were proposed. In this section, we focus on reviewing studies done using SAS since it is a less familiar area compared with XRD. SAS has been used to probe changes in surface roughness, pore sizes, aggregation and coalescence of microfibrils, solution structures of lignin, lignin aggregation, phase separation, etc. during biomass pretreatment. These studies offer important insight into biomass pretreatment and recalcitrance and will be detailed below. Summary of these studies are referenced and listed in Table 1.

SAXS was used in a study investigating the effect of solvent exchange on the pore structure in soft wood dissolving pulp and Whatman filter paper.⁹² Values of specific surface and average chord length calculated from SAXS profile suggested that the amount of small pores with the radii of less than 1 nm increased after *N,N*-dimethylacetamide and acetone treatment.⁹²

Spruce wood was subjected to extraction treatment with sodium chlorite for delignification and with sodium hydroxide for extraction of hemicelluloses.⁷⁰ The corresponding changes to the cell wall structures were investigated by SAXS and WAXS. In that work, the Porod length representing the mean chord length characterizing a typical length scale in two-phase system was calculated using SAXS data.⁷⁰ Jungnikl et al. enabled a qualitative discussion of the changes in the observed Porod length that provided insight into the structural changes that occurred. On the length scale of 6-30 nm, there were no signs of microfibril aggregation or ordered packing for both untreated and delignified samples. The Porod length extracted from the wet samples remained the same after delignification. After additional treatment with 6% NaOH, the Porod length increased strongly. The treatment with NaOH removed lignin residues and parts of the xylan, leaving wider interfibrillar spaces absorbing more water. With further extraction of hemicelluloses, the matrix was dominated by microfibrils and the Porod length started to decrease.⁷⁰ This work is perhaps one of the few earliest studies that focused on the phase separation among cellulose, hemicelluloses and lignin in cell walls during chemical pretreatment.

The impact of surfactants and biopolymers on the mesoscopic structure of cotton fibres was studied using SANS.¹⁴⁵ The shoulder on scattering curve in the region of $\sim 0.1 \text{ \AA}^{-1}$ was attributed to that of cylindrical structures in cotton fibres. At low q , the scattering was due to larger fibrillar superstructure. The radius of the cylindrical structures was determined to be around 5.5 nm. It was found that the addition of anionic surfactants did not affect the local structure of cotton.¹⁴⁵

During past several years, there has been an increase in the number of publications investigating morphological changes of the plant cell walls during biomass pretreatment.²² Switchgrass samples were pretreated with dilute sulphuric acid at 160°C for

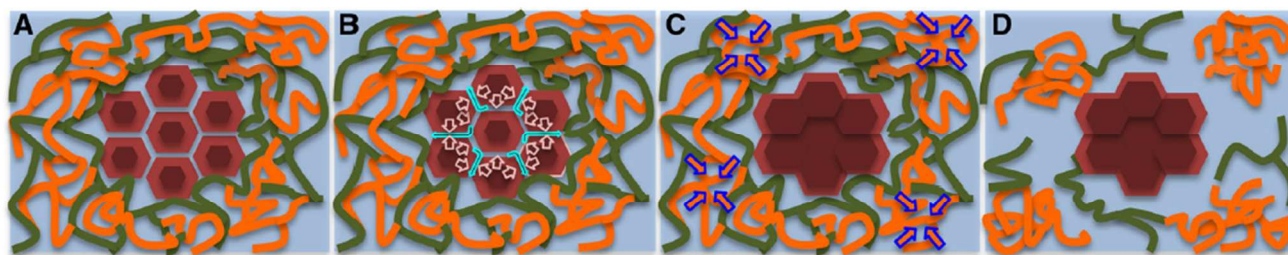


Figure 17. A schematic summarizing the internal structural changes that biomass undergoes during steam explosion pretreatment process. The different panels represents the different phases of the process: a native; b heating; c holding and cool down and d pretreated⁵⁰

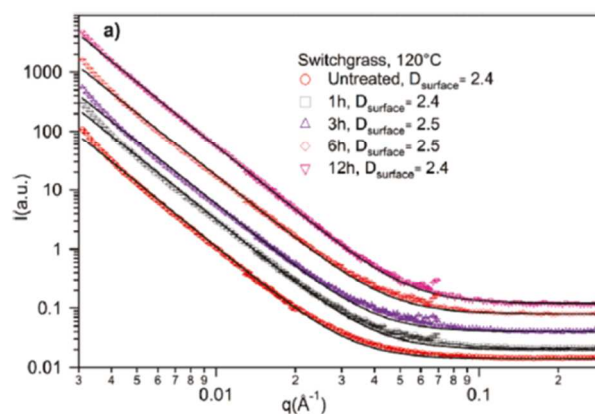
different time periods to investigate structural changes that occur during pretreatment.⁵³ SANS data were collected over a q range of 0.001 to 0.3 \AA^{-1} . The SANS data were interpreted as arising three different structures: diameter of microfibrils (high q), lignin aggregates or branched biomass network (intermediate q) and cell wall surfaces (low q). Pingali et al. found that dilute acid (DA) pretreatment increased the diameters of cellulose microfibrils. They argued that this increase in size was caused by increased packing of microfibrils, as reported by other researchers. The most pronounced change in the SANS data was the presence of a new characteristic length scale which was attributed to lignin aggregates. This finding was consistent with prior studies where DA pretreatment at higher temperatures led to formation of lignin droplet on the surface of cell walls.⁵³

Quaking aspen chips were subjected to different thermochemical pretreatment techniques: dilute acids, AFEX and steam explosion.^{38, 50, 51} Changes in cell wall structures were analyzed by SANS, SAXS and WAXS (fiber diffraction). Langan et al. discovered two fundamental processes responsible for the morphological changes in biomass during thermochemical pretreatment: cellulose dehydration and lignin/hemicelluloses phase separation.³⁸ The results suggested that coalescences of cellulose microfibrils into larger ones as water was released into the surrounding matrix in a thermodynamically entropy-driven process (Figure 17). A more detailed study by Nishiyama et al supported this conclusion.⁵¹ At higher temperatures and pressures, lignin aggregated into crumpled globules with some loss of hemicelluloses through auto-hydrolysis (Figure 17). When the temperature was brought back to room temperature, lignin globules collapsed and phase separated from hemicelluloses. The same group also performed an in situ SANS study of morphological changes to the different components of lignocellulosic biomass during steam pretreatment by placing a pressure reaction cell in a neutron beam and collecting time-resolved neutron scattering data.⁵⁰ Their experimental results further supported that the lignin/hemicelluloses phase separated during thermochemical pretreatment.⁵⁰

SANS was used to investigate the effect of ionic liquid pretreatment on the surface morphology of biomass samples.^{52, 54, 146} Switchgrass, pine, and eucalyptus samples were pretreated in 1-ethyl-3-methyl imidazolium acetate ([C2mim][OAc]) at 120°C over a period of 1 to 12 hours.⁵² In the dry state, all SANS curves follow a power law function in the q range of 0.1 to 0.004 \AA^{-1}

(Figure 18). The power law scattering probes the surface of biomass samples, where its roughness is measured by a surface fractal dimension, $D_{\text{surface}} = 6 - \alpha$, where α is the power law exponent obtained from the scattering data. The variations of surface roughness as a function of pretreatment severity were correlated with delignification and transformation of cellulose crystalline structures. Cheng et al. proposed that partial disruption of cellulose I and delignification of biomass samples results in increased surface roughness, whereas the formation of cellulose II after regeneration results in smoother surfaces.⁵²

In a comparative study between the effects of IL and AFEX pretreatment on the morphology of corn stover samples, SANS curves also follow a single power law function in the q range of $0.1-0.004 \text{ \AA}^{-1}$.⁵⁴ After AFEX, SANS data indicated increased roughness of the internal surfaces. This is in concert with observations of lignin and hemicellulose redistribution on the surface reported elsewhere.³⁹ On the other hand, the surface roughness dropped for the IL pretreated sample, indicating that the regeneration process after IL pretreatment resulted in the formation of smoother internal surfaces. This is due to formation of cellulose II in the IL pretreated samples, consistent with the earlier study.⁵² We do want to note that the resultant cellulose structure upon IL pretreatment is dependent on the nature of IL used.



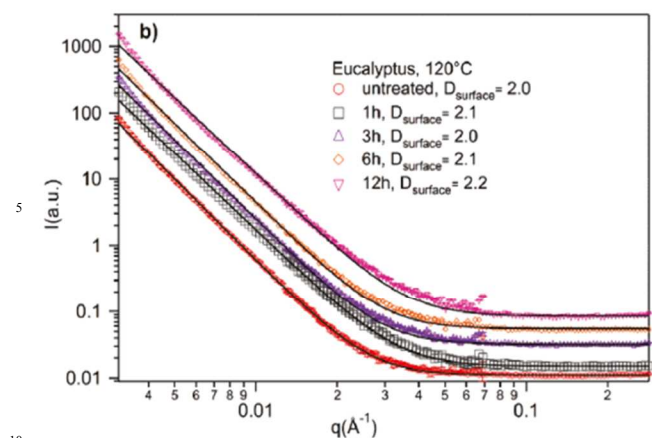


Figure 18 SANS data of (a) switchgrass and (b) eucalyptus samples pretreated in [C2mim][OAc] at 120°C for 1, 3, 6, and 12 h. The solid line is a fit to a power law function, $I(q) = Aq^\alpha + B$.⁵²

In order to reveal additional internal structures within the biomass samples, SANS was also collected on hydrated samples.⁵⁴ All the samples were kept in D₂O for 36 h prior to the measurement to enhance the contrast and lower the background signal. For the untreated sample, excess scattering is present in the q range of 0.1–0.3 Å⁻¹ due to hydration of small pores with a diameter of about 2 nanometres (Figure 19). For the AFEX and IL pretreated samples, the SANS profiles did not show evidences of small pores with a well-defined size distribution. The data indicated a drastic change in the size distribution of the pores and the pores grew in size and coalesced to form larger pores after the pretreatment.⁵⁴

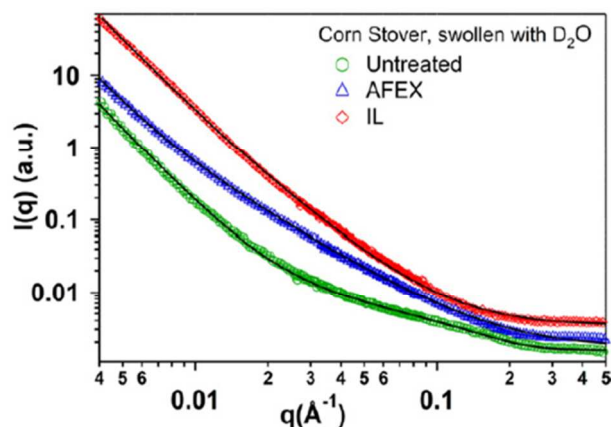


Figure 19 SANS data of corn stover samples in the wet state before and after AFEX and IL pretreatment.⁵⁴

The impact of ionic liquid pretreatment on the structures of lignin in solution was also studied using SANS.⁹⁴ Lignin contains a substantial amount of nanometre scale individual subunits. After the IL treatment individual subunits were released via dissociation or depolymerization, depending on the nature of the interactions among the lignin subunits in the aggregates as well as type of lignin (Figure 20).⁹⁴

Xu et al. used synchrotron WAXS and SAXS to measure structural changes of sorghum after biomass pretreatment.^{69, 147} The 2D SAXS pattern of untreated sample appeared as diamond-

shaped streak elongated on the equator (Figure 21). The equatorial streak was attributed to the presence of microvoids orientated along the fibre axis. The meridional scattering was assigned to scattering from the periodic interval along the microfibril.^{69, 147} After the alkali pretreatment, the diamond-shaped pattern transformed into an isotropic scattering pattern, indicating a decrease in orientation and length of microvoids (Figure 21).¹⁴⁷ In related work, Xu et al. analyzed the size of the microvoids and found that total volume increased after dilute acid pretreatment.⁶⁹ This was correlated with removal of hemicelluloses by acid pretreatment.⁶⁹

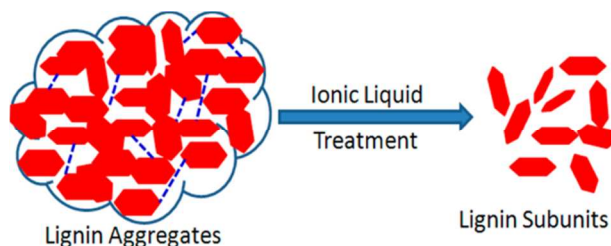


Figure 20 Lignin aggregates consists of nanometer-sized subunits which are released during IL pretreatment⁹⁴

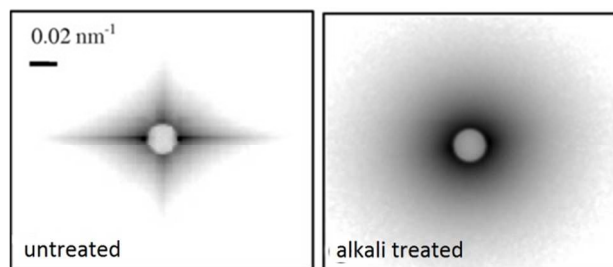


Figure 21 SAXS patterns of untreated and alkali treated sorghum¹⁴⁷

7. Conclusions and future prospects

In this manuscript, we analyzed the most recent literatures on biomass pretreatment and biomass recalcitrance, and focused on hierarchical structures of plant cell wall and their correlations with biomass recalcitrance on the nano/micrometer scale. Besides traditional techniques such as cell wall profiling using wet chemistry, the reorganization of structural features on the nano/micrometer scale during biomass pretreatment is vital to understand the mechanism of the pretreatment process and the nature of biomass recalcitrance. As nano-composites, the integrity of plant cell walls is maintained by interactive interactions among the three major biomacromolecules. Alterations of a specific structure such as a particular inter-linkage will trigger a series of events via either chemical or physical interactions. Structural characterizations on the length scale of cell walls are necessary to describe the effects of biomass pretreatment on the recalcitrant structures in plant cell walls. In conjunction with imaging techniques, WAS and SAS are valuable tools to provide a more complete picture of morphological changes during biomass pretreatment.

In addition to the different applications we summarized in this review article, two additional topics are detailed below that are

suitable for SAS studies of lignocellulosic biomass and should be explored;

1. In-situ measurement of structural changes during biomass pretreatment provides rich dynamic information and is crucial for a better control of pretreatment conditions. Structural information such as MFA, microfibril aggregation and reorganization, lignin aggregation and phase separation can be obtained with SAS studies.

2. In-situ measurement of structural changes during enzymatic digestion of biomass samples. Although there have been a few studies on this topic by SANS/SAXS, more work is needed to probe these interactions since the nature of cellulases and solid substrate interactions are complex. Advances in data analysis methods are also needed to improve our current understanding of cellulases and solid substrate interactions. On the other hand, highlighting a particular structure by deuteration and contrast enhancing in neutron scattering experiments will reduce the complex structure of plant biomass to a simpler one and will aid in the data analysis.

We want to emphasize that analysis of SAS from lignocellulosic biomass samples is not trivial. For example, whether the SAS data in the higher q region (around 0.1 \AA^{-1}) is due to scattering from cross-section of microfibrils or nanometre-sized pores, or both, need to be analyzed with caution. Variations of the SAS data with hydration cannot differentiate the scattering from pores or microfibrils as both the sizes of the pores and the inter-fibrillar distances can change. This is also the case for analysis of 2D SAS data. The equatorial streak has been attributed to the presence of microvoids or microfibrils orientated along the fibre axis. The meridional scattering has been interpreted as scattering objects with a lower aspect ratio, from microfibrils in S1/S3 layer or the periodic interval along the microfibrils.

For those who are interested in using scattering techniques, especially SAS, to study the structure of biomass samples, collaborative discussions with instrument scientist are important and encouraged. Data analysis software is usually provided by the different facilities. One such example can be found on this website: <http://sasview.org/>, where the SAS analysis software is available for free. Tutorial courses on x-ray and neutron scattering are offered annually by different institutions, for example, National school on X-ray and neutron scattering (<http://neutrons.ornl.gov/nxs/>) by Oak Ridge National Laboratory and Argonne National Laboratory, summer school on the fundamentals of neutron scattering (<http://www.ncnr.nist.gov/summerschool/>) by National Institute of Standard and Technology, Oxford School on neutron scattering (<http://www.oxfordneutronschool.org/>) by Oxford University, etc. Our hope is that both, experts of WAS and SAS who are unfamiliar with lignocellulosic biomass, as well as plant and biofuels experts who are unfamiliar with WAS and SAS will benefit from this review article and that they seek out powerful collaborations and new approaches overcoming some of the current limitations of these tools to further this important field of research and development to enable lignocellulosic biofuels and bioproducts.

Acknowledgements

This journal is © The Royal Society of Chemistry [year]

We gratefully acknowledge support for this research by the Office of Biological and Environmental Research in the DOE Office of Science through the Joint BioEnergy Institute (JBEI) (Grant DE-AC02-05CH11231). Gang Cheng acknowledges support for this research by the National Natural Science Foundation of China (U1432109).

Notes

⁶⁵ ^a Beijing Key Laboratory of Bioprocess and College of Life Science and Technology, Beijing University of Chemical Technology, Beijing, 100029, China. Tel: 86-13693276690; E-mail: chenggang@mail.buct.edu.cn

^b Deconstruction Division, Joint BioEnergy Institute (JBEI), Emeryville, CA 94608, USA E-mail: singh@lbl.gov

⁷⁰ ^c Sandia National Laboratories, Livermore, CA 94551, USA

* Corresponding authors: Gang Cheng and Seema Singh

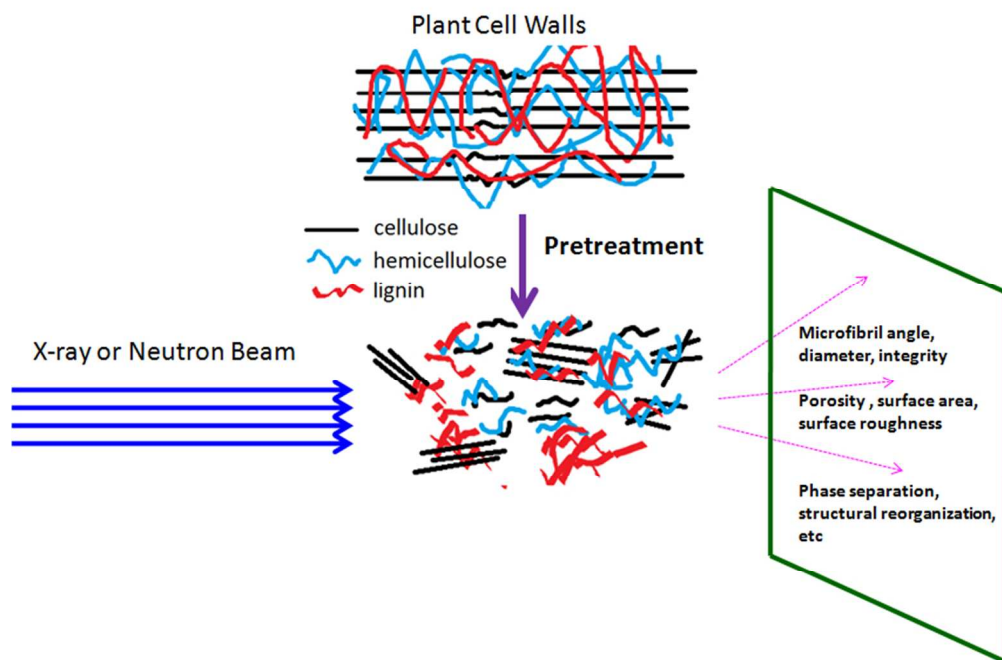
References

1. V. Menon and M. Rao, *Progress in Energy and Combustion Science*, 2012, **38**, 522-550.
2. C. Somerville and H. Youngs, *Biotechnology and Bioengineering*, 2014, **111**, 1717-1718.
3. H. R. Bungay, *Science*, 1982, **218**, 643-646.
4. C. Somerville, H. Youngs, C. Taylor, S. C. Davis and S. P. Long, *Science*, 2010, **329**, 790-792.
5. F. Peng, P. Peng, F. Xu and R.-C. Sun, *Biotechnology Advances*, 2012, **30**, 879-903.
6. K. E. Achyuthan, A. M. Achyuthan, P. D. Adams, S. M. Dirk, J. C. Harper, B. A. Simmons and A. K. Singh, *Molecules*, 2010, **15**, 8641-8688.
7. A. J. Ragauskas, G. T. Beckham, M. J. Bidy, R. Chandra, F. Chen, M. F. Davis, B. H. Davison, R. A. Dixon, P. Gilna, M. Keller, P. Langan, A. K. Naskar, J. N. Saddler, T. J. Tschaplinski, G. A. Tuskan and C. E. Wyman, *Science*, 2014, **344**.
8. D. Chiramonti, M. Prussi, S. Ferrero, L. Oriani, P. Ottonello, P. Torre and F. Cherchi, *Biomass and Bioenergy*, 2012, **46**, 25-35.
9. A. Limayem and S. C. Ricke, *Progress in Energy and Combustion Science*, 2012, **38**, 449-467.
10. P. J. Harris and B. A. Stone, in *Biomass Recalcitrance*, Blackwell Publishing Ltd., 2009, pp. 61-93.
11. M. Foston and A. J. Ragauskas, *Industrial Biotechnology*, 2012, **8**, 191-208.
12. H. Rasmussen, H. R. Sørensen and A. S. Meyer, *Carbohydrate Research*, 2014, **385**, 45-57.
13. X. Meng and A. J. Ragauskas, *Current Opinion in Biotechnology*, 2014, **27**, 150-158.
14. D. Klein-Marcuschamer, P. Oleskowicz-Popiel, B. A. Simmons and H. W. Blanch, *Biotechnology and Bioengineering*, 2012, **109**, 1083-1087.
15. Y. Pu, F. Hu, F. Huang, B. Davison and A. Ragauskas, *Biotechnology for Biofuels*, 2013, **6**, 15.
16. S. Behera, R. Arora, N. Nandhagopal and S. Kumar, *Renewable and Sustainable Energy Reviews*, 2014, **36**, 91-106.
17. Y. Zheng, J. Zhao, F. Xu and Y. Li, *Progress in Energy and Combustion Science*, 2014, **42**, 35-53.

18. D. Carpenter, T. L. Westover, S. Czernik and W. Jablonski, *Green Chemistry*, 2014, **16**, 384-406.
19. S. Haghghi Mood, A. Hossein Golfeshan, M. Tabatabaei, G. Salehi Jouzani, G. H. Najafi, M. Gholami and M. Ardjmand, *Renewable and Sustainable Energy Reviews*, 2013, **27**, 77-93.
20. R. Singh, A. Shukla, S. Tiwari and M. Srivastava, *Renewable and Sustainable Energy Reviews*, 2014, **32**, 713-728.
21. D. Bacovsky, N. Ludwiczek, M. Ognissanto and M. Wörgetter, http://demoplants.bioenergy2020.eu/files/Demoplants_Report_Final.pdf, 2013.
22. M. S. Singhvi, S. Chaudhari and D. V. Gokhale, *RSC Advances*, 2014, **4**, 8271-8277.
23. R. Ong, S. S. Chundawat, D. Hodge, S. Keskar and B. Dale, in *Plants and BioEnergy*, eds. M. C. McCann, M. S. Buckeridge and N. C. Carpita, Springer New York, 2014, vol. 4, ch. 14, pp. 231-253.
24. J. D. DeMartini, S. Pattathil, J. S. Miller, H. Li, M. G. Hahn and C. E. Wyman, *Energy & Environmental Science*, 2013, **6**, 898-909.
25. X. Zhao, L. Zhang and D. Liu, *Biofuels, Bioproducts and Biorefining*, 2012, **6**, 465-482.
26. R. Van Acker, R. Vanholme, V. Storme, J. Mortimer, P. Dupree and W. Boerjan, *Biotechnology for Biofuels*, 2013, **6**, 46.
27. F. Chen and R. A. Dixon, *Nat Biotech*, 2007, **25**, 759-761.
28. F. Yang, P. Mitra, L. Zhang, L. Prak, Y. Verhertbruggen, J.-S. Kim, L. Sun, K. Zheng, K. Tang, M. Auer, H. V. Scheller and D. Loqué, *Plant Biotechnology Journal*, 2013, **11**, 325-335.
29. S. L. Voelker, B. Lachenbruch, F. C. Meinzer, M. Jourdes, C. Ki, A. M. Patten, L. B. Davin, N. G. Lewis, G. A. Tuskan, L. Gunter, S. R. Decker, M. J. Selig, R. Sykes, M. E. Himmel, P. Kitin, O. Shevchenko and S. H. Strauss, *Plant Physiology*, 2010, **154**, 874-886.
30. J. D. DeMartini, S. Pattathil, U. Avcı, K. Szekalski, K. Mazumder, M. G. Hahn and C. E. Wyman, *Energy & Environmental Science*, 2011, **4**, 4332-4339.
31. N. C. Carpita, *Current Opinion in Biotechnology*, 2012, **23**, 330-337.
32. R. L. Silveira, S. R. Stoyanov, S. Gusarov, M. S. Skaf and A. Kovalenko, *Journal of the American Chemical Society*, 2013, **135**, 19048-19051.
33. D. D. Laskar, B. Yang, H. Wang and J. Lee, *Biofuels, Bioproducts and Biorefining*, 2013, **7**, 602-626.
34. S.-Y. Ding, Y.-S. Liu, Y. Zeng, M. E. Himmel, J. O. Baker and E. A. Bayer, *Science*, 2012, **338**, 1055-1060.
35. F. Xu, Y.-C. Shi and D. Wang, *Carbohydrate Polymers*, 2013, **94**, 904-917.
36. H. Inouye, Y. Zhang, L. Yang, N. Venugopalan, R. F. Fischetti, S. C. Gleber, S. Vogt, W. Fowle, B. Makowski, M. Tucker, P. Ciesielski, B. Donohoe, J. Matthews, M. E. Himmel and L. Makowski, *Sci. Rep.*, 2014, **4**.
37. L. Sun, C. Li, Z. Xue, B. A. Simmons and S. Singh, *RSC Advances*, 2013, **3**, 2017-2027.
38. P. Langan, L. Petridis, H. M. O'Neill, S. V. Pingali, M. Foston, Y. Nishiyama, R. Schulz, B. Lindner, B. L. Hanson, S. Harton, W. T. Heller, V. Urban, B. R. Evans, S. Gnanakaran, A. J. Ragauskas, J. C. Smith and B. H. Davison, *Green Chemistry*, 2014, **16**, 63-68.
39. S. P. S. Chundawat, B. S. Donohoe, L. da Costa Sousa, T. Elder, U. P. Agarwal, F. Lu, J. Ralph, M. E. Himmel, V. Balan and B. E. Dale, *Energy & Environmental Science*, 2011, **4**, 973-984.
40. M. J. Selig, S. Viamajala, S. R. Decker, M. P. Tucker, M. E. Himmel and T. B. Vinzant, *Biotechnology Progress*, 2007, **23**, 1333-1339.
41. B. S. Donohoe, S. R. Decker, M. P. Tucker, M. E. Himmel and T. B. Vinzant, *Biotechnology and Bioengineering*, 2008, **101**, 913-925.
42. R. Ibbett, S. Gaddipati, S. Hill and G. Tucker, *Biotechnology for Biofuels*, 2013, **6**, 33.
43. H. F. Jakob, D. Fengel, S. E. Tschegg and P. Fratzl, *Macromolecules*, 1995, **28**, 8782-8787.
44. C. Kennedy, G. Cameron, A. Šturcová, D. Apperley, C. Altaner, T. Wess and M. Jarvis, *Cellulose*, 2007, **14**, 235-246.
45. K. Leppänen, S. Andersson, M. Torkkeli, M. Knaapila, N. Kotelnikova and R. Serimaa, *Cellulose*, 2009, **16**, 999-1015.
46. J. Fahlén and L. Salmén, *Biomacromolecules*, 2004, **6**, 433-438.
47. S. Singh, B. A. Simmons and K. P. Vogel, *Biotechnology and Bioengineering*, 2009, **104**, 68-75.
48. M. Foston, *Current Opinion in Biotechnology*, 2014, **27**, 176-184.
49. Y. Pu, S. Cao and A. J. Ragauskas, *Energy & Environmental Science*, 2011, **4**, 3154-3166.
50. S. Pingali, H. O'Neill, Y. Nishiyama, L. He, Y. Melnichenko, V. Urban, L. Petridis, B. Davison and P. Langan, *Cellulose*, 2014, **21**, 873-878.
51. Y. Nishiyama, P. Langan, H. O'Neill, S. Pingali and S. Harton, *Cellulose*, 2014, **21**, 1015-1024.
52. G. Cheng, P. Varanasi, C. Li, H. Liu, Y. B. Melnichenko, B. A. Simmons, M. S. Kent and S. Singh, *Biomacromolecules*, 2011, **12**, 933-941.
53. S. V. Pingali, V. S. Urban, W. T. Heller, J. McGaughey, H. O'Neill, M. Foston, D. A. Myles, A. Ragauskas and B. R. Evans, *Biomacromolecules*, 2010, **11**, 2329-2335.
54. C. Li, G. Cheng, V. Balan, M. S. Kent, M. Ong, S. P. S. Chundawat, L. d. Sousa, Y. B. Melnichenko, B. E. Dale, B. A. Simmons and S. Singh, *Bioresour. Technol.*, 2011, **102**, 6928-6936.
55. P. Langan, B. R. Evans, M. Foston, W. T. Heller, H. O'Neill, L. Petridis, S. V. Pingali, A. Ragauskas, J. C. Smith, V. Urban and B. H. Davidson, *Industrial Biotechnology*, 2012, **8**, 209-216.
56. R. J. Roe, *Methods of X-ray and Neutron Scattering in Polymer Science*, Oxford University Press, 2000.
57. J. Sugiyama, R. Vuong and H. Chanzy, *Macromolecules*, 1991, **24**, 4168-4175.
58. Y. Nishiyama, J. Sugiyama, H. Chanzy and P. Langan, *Journal of the American Chemical Society*, 2003, **125**, 14300-14306.
59. C. Driemeier and G. A. Calligaris, *Journal of Applied Crystallography*, 2011, **44**, 184-192.
60. S. Park, J. Baker, M. Himmel, P. Parilla and D. Johnson, *Biotechnology for Biofuels*, 2010, **3**, 10.
61. A. O'Sullivan, *Cellulose*, 1997, **4**, 173-207.
62. P. Langan, Y. Nishiyama and H. Chanzy, *Journal of the American Chemical Society*, 1999, **121**, 9940-9946.

63. S. P. S. Chundawat, G. Bellesia, N. Uppugundla, L. da Costa Sousa, D. Gao, A. M. Cheh, U. P. Agarwal, C. M. Bianchetti, G. N. Phillips, P. Langan, V. Balan, S. Gnanakaran and B. E. Dale, *Journal of the American Chemical Society*, 2011, **133**, 11163-11174.
64. H. Liu, G. Cheng, M. Kent, V. Stavila, B. A. Simmons, K. L. Sale and S. Singh, *The Journal of Physical Chemistry B*, 2012, **116**, 8131-8138.
65. H. Lichtenegger, A. Reiterer, S. E. Tschegg and P. Fratzl, in *Microfibril angle in wood*, ed. B. G. Butterfield, University of Canterbury, 1998.
66. M. De Spirito, M. Missori, M. Papi, G. Maulucci, J. Teixeira, C. Castellano and G. Arcovito, *Physical Review E*, 2008, **77**, 041801.
67. M. S. Kent, G. Cheng, J. K. Murton, E. L. Carles, D. C. Dibble, F. Zendejas, M. A. Rodriguez, H. Tran, B. Holmes, B. A. Simmons, B. Knierim, M. Auer, J. L. Banuelos, J. Urquidi and R. P. Hjelm, *Biomacromolecules*, 2009, **11**, 357-368.
68. P. Penttilä, A. Várnai, M. Fernández, I. Kontro, V. Liljeström, P. Lindner, M. Siika-aho, L. Viikari and R. Serimaa, *Cellulose*, 2013, **20**, 1031-1040.
69. F. Xu, Y.-C. Shi and D. Wang, *Bioresource Technology*, 2013, **135**, 704-709.
70. K. Jungnikl, O. Paris, P. Fratzl and I. Burgert, *Cellulose*, 2008, **15**, 407-418.
71. G. Cheng, Z. Liu, J. K. Murton, M. Jablin, M. Dubey, J. Majewski, C. Halbert, J. Browning, J. Ankner, B. Akgun, C. Wang, A. R. Esker, K. L. Sale, B. A. Simmons and M. S. Kent, *Biomacromolecules*, 2011, **12**, 2216-2224.
72. H. F. Jakob, S. E. Tschegg and P. Fratzl, *Macromolecules*, 1996, **29**, 8435-8440.
73. O. Paris, *Biointerphases*, 2008, **3**, FB16-FB26.
74. A. Reiterer, H. F. Jakob, S. E. Stanzl-Tschegg and P. Fratzl, *Wood Sci. Technol.*, 1998, **32**, 335-345.
75. P. Schmidt, *Journal of Applied Crystallography*, 1991, **24**, 414-435.
76. N. Hu, N. Borkar, D. Kohls and D. W. Schaefer, *Journal of Membrane Science*, 2011, **379**, 138-145.
77. C. R. Clarkson, N. Solano, R. M. Bustin, A. M. M. Bustin, G. R. L. Chalmers, L. He, Y. B. Melnichenko, A. P. Radliński and T. P. Blach, *Fuel*, 2013, **103**, 606-616.
78. G. Cheng, P. Varanasi, R. Arora, V. Stavila, B. A. Simmons, M. S. Kent and S. Singh, *The Journal of Physical Chemistry B*, 2012, **116**, 10049-10054.
79. M. J. Hollamby, *Physical Chemistry Chemical Physics*, 2013, **15**, 10566-10579.
80. I. D. Cave, *Wood Sci. Technol.*, 1997, **31**, 143-152.
81. M.-P. Sarén, R. Serimaa, S. Andersson, P. Saranpää, J. Keckes and P. Fratzl, *Trees*, 2004, **18**, 354-362.
82. I. D. Cave, *Wood Sci. Technol.*, 1997, **31**, 225-234.
83. S. Andersson, R. Serimaa, M. Torkkeli, T. Paakkari, P. Saranpää and E. Pesonen, *J Wood Sci*, 2000, **46**, 343-349.
84. H. Suzuki and T. Kamiyama, *J Wood Sci*, 2004, **50**, 351-357.
85. P. A. Penttilä, A. Várnai, K. Leppänen, M. Peura, A. Kallonen, P. Jääskeläinen, J. Lucenius, J. Ruokolainen, M. Siika-aho, L. Viikari and R. Serimaa, *Biomacromolecules*, 2010, **11**, 1111-1117.
86. G. Sèbe, F. Ham-Pichavant, E. Ibarboure, A. L. C. Koffi and P. Tingaut, *Biomacromolecules*, 2012, **13**, 570-578.
87. E. W. Fischer, P. Herchenröder, R. S. J. Manley and M. Stamm, *Macromolecules*, 1978, **11**, 213-217.
88. Y. Nishiyama, U.-J. Kim, D.-Y. Kim, K. S. Katsumata, R. P. May and P. Langan, *Biomacromolecules*, 2003, **4**, 1013-1017.
89. T. Paakkari and R. Serimaa, *Wood Sci. Technol.*, 1984, **18**, 79-85.
90. U. Vainio, S. Andersson, R. Serimaa, T. Paakkari, P. Saranpää, M. Treacy and J. Evertsen, *Plant Biology*, 2002, **4**, 27-33.
91. J. Färber, H. C. Lichtenegger, A. Reiterer, S. Stanzl-Tschegg and P. Fratzl, *Journal of Materials Science*, 2001, **36**, 5087-5092.
92. D. Ishii, Y. Kanazawa, D. Tatsumi and T. Matsumoto, *Journal of Applied Polymer Science*, 2007, **103**, 3976-3984.
93. U. Vainio, R. A. Lauten and R. Serimaa, *Langmuir*, 2008, **24**, 7735-7743.
94. G. Cheng, M. S. Kent, L. He, P. Varanasi, D. Dibble, R. Arora, K. Deng, K. Hong, Y. B. Melnichenko, B. A. Simmons and S. Singh, *Langmuir*, 2012, **28**, 11850-11857.
95. S. E. Harton, S. V. Pingali, G. A. Nunnery, D. A. Baker, S. H. Walker, D. C. Muddiman, T. Koga, T. G. Rials, V. S. Urban and P. Langan, *ACS Macro Letters*, 2012, **1**, 568-573.
96. G. Cheng, S. Datta, Z. Liu, C. Wang, J. K. Murton, P. A. Brown, M. S. Jablin, M. Dubey, J. Majewski, C. E. Halbert, J. F. Browning, A. R. Esker, B. J. Watson, H. Zhang, S. W. Hutcheson, D. L. Huber, K. L. Sale, B. A. Simmons and M. S. Kent, *Langmuir*, 2012, **28**, 8348-8358.
97. V. Reyes-Ortiz, R. Heins, G. Cheng, E. Kim, B. Vernon, R. Elandt, P. Adams, K. Sale, M. Hadi, B. Simmons, M. Kent and D. Tullman-Ercek, *Biotechnology for Biofuels*, 2013, **6**, 93.
98. H. Lichtenegger, A. Reiterer, S. E. Stanzl-Tschegg and P. Fratzl, *Journal of Structural Biology*, 1999, **128**, 257-269.
99. R. M. Brown and D. Montezinos, *Proceedings of the National Academy of Sciences*, 1976, **73**, 143-147.
100. S. M. Read and T. Bacic, *Science*, 2002, **295**, 59-60.
101. R. J. Moon, A. Martini, J. Nairn, J. Simonsen and J. Youngblood, *Chemical Society Reviews*, 2011, **40**, 3941-3994.
102. S. Elazzouzi-Hafraoui, Y. Nishiyama, J.-L. Putaux, L. Heux, F. Dubreuil and C. Rochas, *Biomacromolecules*, 2007, **9**, 57-65.
103. A. N. Fernandes, L. H. Thomas, C. M. Altaner, P. Callow, V. T. Forsyth, D. C. Apperley, C. J. Kennedy and M. C. Jarvis, *Proceedings of the National Academy of Sciences*, 2011, **108**, E1195-E1203.
104. M.-A. Ha, D. C. Apperley, B. W. Evans, I. M. Huxham, W. G. Jardine, R. J. Viëtor, D. Reis, B. Vian and Michael C. Jarvis, *The Plant Journal*, 1998, **16**, 183-190.
105. L. H. Thomas, V. T. Forsyth, A. Šturcová, C. J. Kennedy, R. P. May, C. M. Altaner, D. C. Apperley, T. J. Wess and M. C. Jarvis, *Plant Physiology*, 2013, **161**, 465-476.
106. A.-C. Engström, M. Ek and G. Henriksson, *Biomacromolecules*, 2006, **7**, 2027-2031.
107. Y. Habibi, L. A. Lucia and O. J. Rojas, *Chemical Reviews*, 2010, **110**, 3479-3500.

- 108.M. M. De Souza Lima, J. T. Wong, M. Paillet, R. Borsali and R. Pecora, *Langmuir*, 2002, **19**, 24-29.
- 109.P. Terech, L. Chazeau and J. Y. Cavaille, *Macromolecules*, 1999, **32**, 1872-1875.
- 5 110.P. B. Filson and B. E. Dawson-Andoh, *Bioresource Technology*, 2009, **100**, 2259-2264.
- 111.N. Johar, I. Ahmad and A. Dufresne, *Industrial Crops and Products*, 2012, **37**, 93-99.
- 112.Z. Lu, L. Fan, H. Zheng, Q. Lu, Y. Liao and B. Huang, *Bioresource Technology*, 2013, **146**, 82-88.
- 10 113.S. Mueller, C. Weder and E. J. Foster, *RSC Advances*, 2014, **4**, 907-915.
- 114.M. Martínez-Sanz, A. Lopez-Rubio and J. M. Lagaron, *Carbohydrate Polymers*, 2011, **85**, 228-236.
- 115.L. Brinchi, F. Cotana, E. Fortunati and J. M. Kenny, *Carbohydrate Polymers*, 2013, **94**, 154-169.
- 116.P. B. Filson, B. E. Dawson-Andoh and D. Schwegler-Berry, *Green Chemistry*, 2009, **11**, 1808-1814.
- 117.P. Satyamurthy and N. Vigneshwaran, *Enzyme and Microbial Technology*, 2013, **52**, 20-25.
- 20 118.G. Siqueira, S. Tapin-Lingua, J. Bras, D. da Silva Perez and A. Dufresne, *Cellulose*, 2010, **17**, 1147-1158.
- 119.M. Chauve, L. Barre, S. Tapin-Lingua, D. Silva Perez, D. Decottignies, S. Perez and N. L. Ferreira, *Advances in Bioscience and Biotechnology*, 2013, **4**, 1095-1109.
- 25 120.G. Neutelings, *Plant Science*, 2011, **181**, 379-386.
- 121.M. P. Pandey and C. S. Kim, *Chemical Engineering & Technology*, 2011, **34**, 29-41.
- 122.A. P. Karmanov and Y. B. Monakov, *ChemInform*, 2004, **35**, no-no.
- 30 123.C. Crestini, F. Melone, M. Sette and R. Saladino, *Biomacromolecules*, 2011, **12**, 3928-3935.
- 124.D. Lairez, B. Cathala, B. Monties, F. Bedos-Belval, H. Duran and L. Gorrichon, *Biomacromolecules*, 2005, **6**, 763-774.
- 125.K. Radotić, M. Mičić and M. Jeremić, *Annals of the New York Academy of Sciences*, 2005, **1048**, 215-229.
- 35 126.G. Gilardi and A. E. G. Cass, *Langmuir*, 1993, **9**, 1721-1726.
- 127.M. Norgren, H. Edlund and L. Wagberg, *Langmuir*, 2002, **18**, 2859-2865.
- 128.A. V. Gidh, S. R. Decker, T. B. Vinzant, M. E. Himmel and C. Williford, *J Chromatogr A*, 2006, **1114**, 102-110.
- 40 129.A. V. Gidh, S. R. Decker, C. H. See, M. E. Himmel and C. W. Williford, *Anal Chim Acta*, 2006, **555**, 250-258.
- 130.S. Contreras, A. R. Gaspar, A. Guerra, L. A. Lucia and D. S. Argyropoulos, *Biomacromolecules*, 2008, **9**, 3362-3369.
- 45 131.X. Q. Qui, Q. A. Kong, M. S. Zhou and D. J. Yang, *J Phys Chem B*, 2010, **114**, 15857-15861.
- 132.M. F. Yan, D. J. Yang, Y. H. Deng, P. Chen, H. F. Zhou and X. Q. Qiu, *Colloid Surface A*, 2010, **371**, 50-58.
- 133.A. Guerra, A. R. Gaspar, S. Contreras, L. A. Lucia, C. Crestini and D. S. Argyropoulos, *Phytochemistry*, 2007, **68**, 2570-2583.
- 50 134.U. Vainio, N. Maximova, B. Hortling, J. Laine, P. Stenius, L. K. Simola, J. Gravitis and R. Serimaa, *Langmuir*, 2004, **20**, 9736-9744.
- 135.J. Y. Kim, E. J. Shin, I. Y. Eom, K. Won, Y. H. Kim, D. Choi, I. G. Choi and J. W. Choi, *Bioresource Technology*, 2011, **102**, 9020-9025.
- 55 136.W. Lan, C. F. Liu and R. G. Sun, *Journal of Agricultural and Food Chemistry*, 2011, **59**, 8691-8701.
- 137.J. Crawshaw and R. E. Cameron, *Polymer*, 2000, **41**, 4691-4698.
- 60 138.J. Crawshaw, W. Bras, G. R. Mant and R. E. Cameron, *Journal of Applied Polymer Science*, 2002, **83**, 1209-1218.
- 139.X. Chen, C. Burger, F. Wan, J. Zhang, L. Rong, B. S. Hsiao, B. Chu, J. Cai and L. Zhang, *Biomacromolecules*, 2007, **8**, 1918-1926.
- 140.S. Fischer, T. Diesner, B. Rieger and O. Marti, *Journal of Applied Crystallography*, 2010, **43**, 603-610.
- 65 141.D. Capitani, N. Proietti, F. Ziarelli and A. L. Segre, *Macromolecules*, 2002, **35**, 5536-5543.
- 142.C. I. Ishizawa, M. F. Davis, D. F. Schell and D. K. Johnson, *Journal of Agricultural and Food Chemistry*, 2007, **55**, 2575-2581.
- 70 143.Y. Zhang, B. Xu and W. Zhou, *Biotechnology and Bioengineering*, 2014, **111**, 1767-1781.
- 144.P. Bansal, B. J. Vowell, M. Hall, M. J. Realf, J. H. Lee and A. S. Bommarium, *Bioresource Technology*, 2012, **107**, 243-250.
- 145.I. Hoffmann, C. Ooppel, S. Prévost, U. Gernert, P. Barreleiro, W. von Rybinski and M. Gradzielski, *Colloids and Surfaces B: Biointerfaces*, 2012, **91**, 175-180.
- 75 146.Ö. P. Çetinkol, D. C. Dibble, G. Cheng, M. S. Kent, B. Knierim, M. Auer, D. E. Wemmer, J. G. Pelton, Y. B. Melnichenko, J. Ralph, B. A. Simmons and B. M. Holmes, *Biofuels*, 2009, **1**, 33-46.
- 80 147.F. Xu, Y.-C. Shi and D. Wang, *Carbohydrate Polymers*, 2012, **88**, 1149-1156.
- 85



Graphical Table of Contents
225x150mm (96 x 96 DPI)